

1 **Semi-quantitative reconstruction of early to late Holocene spring and summer sea ice**
2 **conditions in the northern Barents Sea**

3

4 **Sarah M.P. Berben^{a,1}, Katrine Husum^b, Alba Navarro-Rodriguez^c, Simon T. Belt^c, Steffen**
5 **Aagaard-Sørensen^a**

6 ^a *Department of Geology, UiT – The Arctic University of Norway, N-9037 Tromsø, Norway*

7 ^b *Norwegian Polar Institute, Fram Centre, N-9296 Tromsø, Norway*

8 ^c *Biogeochemistry Research Centre, School of Geography, Earth and Environmental Sciences,*
9 *University of Plymouth, Drake Circus, Plymouth PL4 8AA, UK*

10

11 ¹Corresponding author.

12 E-mail address: sarah.berben@uib.no

13 Current address: Department of Earth Science, University of Bergen and the Bjerknes Centre
14 for Climate Research, N-5007 Bergen, Norway

15

16 **Abstract**

17 Semi-quantitative estimates of early to late Holocene spring sea ice concentration (SpSIC) and
18 occurrence of summer sea ice for the northern Barents Sea have been obtained by analysing the
19 biomarkers IP₂₅, brassicasterol and a tri-unsaturated highly branched isoprenoid lipid in a
20 Holocene marine sediment core. Sub-surface water mass variations were derived from planktic
21 foraminiferal assemblages and stable isotopes ($\delta^{18}\text{O}$, $\delta^{13}\text{C}$). The record indicates
22 paleoceanographic changes over three intervals. During Period I (ca. 9500–5900 cal a BP), the
23 study location experienced the lowest recorded SpSIC (ca. 25%) with short spring seasons and
24 long productive summers, resulting partly from increased Atlantic Water inflow that caused a
25 stronger ocean-atmosphere heat exchange. Throughout Period II (ca. 5900–2700 cal a BP), the
26 winter sea ice margin migrated southwards and an overall cooling trend resulted in higher
27 SpSIC (ca. 60%) and increased delivery of cold Arctic Water. During Period III (ca. 2700 cal a
28 BP–present), SpSIC increased further (ca. 75%) and some sea ice remained during summer
29 months. A sub-surface warming likely indicates a decoupling of heat exchange between the
30 ocean and the atmosphere. Longer springs and shorter summers were accompanied by the most
31 southerly location of the winter sea ice margin.

32

33 **Keywords**

34 Sea ice, biomarker, proxy data, Holocene, Arctic

35

36 **Introduction**

37 The Barents Sea is a relatively small and shallow sea, yet it plays a crucial role in the Arctic
38 climate system, in part, because of significant heat exchange between the ocean and the
39 atmosphere (Serreze *et al.*, 2007). Oceanic heat is brought into the Barents Sea via the inflow
40 of warm Atlantic water and, due to shallow depths, heat loss to the atmosphere is very efficient.
41 Further, it has been suggested that ocean advection strongly influences sea ice conditions in the
42 Barents Sea, so the region is central to understanding ocean-sea ice-atmosphere interactions
43 (Vinje, 2001).

44 Recently, many Arctic regions have experienced an abrupt decline in sea ice conditions, with
45 the northern Barents Sea and the Chukchi Sea identified as the most affected areas during the
46 last three to four decades (Screen and Simmonds, 2010; Stroeve *et al.*, 2007, 2012). Present day
47 sea ice variations within the Barents Sea have been attributed to different processes (e.g.
48 atmospheric circulation variability, local wind patterns, ice import from the Arctic interior to
49 the Barents Sea), although the role of oceanic heat advection is often emphasized as one of the
50 most important factors (e.g. Årthun *et al.*, 2012; Ivanov *et al.*, 2012; Smedsrud *et al.*, 2013).
51 For example, Årthun *et al.* (2012) argued that recent increases in Atlantic Water inflow to the
52 Barents Sea has contributed to a further decline in sea ice conditions in the Barents Sea.
53 Similarly, the northerly inflow of Pacific Water has been suggested as a contributing factor to
54 reduced sea ice conditions in the Chukchi Sea in recent times (e.g. Shimada *et al.*, 2006;
55 Woodgate *et al.*, 2010) and during the Holocene (Stein *et al.*, 2016a).

56 Since the impacts of Arctic amplification and the associated sea ice decline (Serreze and
57 Francis, 2006; Screen and Simmonds, 2010) reach far beyond the Arctic region (Yang and
58 Christensen, 2012), it is clearly necessary to better understand the interaction between sea ice
59 production and water mass conditions, together with any natural variability that occurs between
60 them over longer time frames. Instrumental and observational records of past climate variations
61 in the Barents Sea reach back only ca. 100–150 years (Divine and Dick, 2006; Smedsrud *et al.*,
62 2013), so longer-term records of sea ice and water mass conditions need to be derived from
63 proxy climate indicators archived in marine sediment cores. Such records from the northern
64 Barents Sea (e.g. Duplessy *et al.*, 2001; Lubinski *et al.*, 2001; Risebrobakken *et al.*, 2011;
65 Klitgaard Kristensen *et al.*, 2013), the western Barents Sea (Berben *et al.*, 2014) and the
66 Svalbard margin (e.g. Slubowska *et al.*, 2005; Rasmussen *et al.*, 2007; Spielhagen *et al.*, 2011;

67 Müller *et al.*, 2012; Werner *et al.*, 2013) have demonstrated various fluctuations of both the
68 influence of Atlantic Water inflow to the Barents Sea and sea ice conditions throughout the
69 Holocene. The observed Holocene changes in the region have mainly been attributed to
70 insolation changes and further factors such as land-cover feedbacks and coupled atmospheric-
71 oceanic dynamics, in particular the northward penetration of relatively warm Atlantic Water
72 (Berger, 1978; Koç *et al.*, 1993; Kaufman *et al.*, 2004). Additionally, insolation forcing has also
73 been attributed to the long-term sea ice variability (Müller *et al.*, 2012; Cabedo-Sanz *et al.*,
74 2016b). However, few of these reconstructions have employed a specific proxy for sea ice or
75 have provided detailed descriptions of sea ice conditions, including semi-quantitative estimates
76 of spring sea ice concentration (SpSIC) or summer sea ice occurrence.

77 In this study, the biomarkers IP₂₅, brassicasterol and a tri-unsaturated highly branched
78 isoprenoid (HBI) lipid (HBI III) have been analyzed in a marine sediment core from the Olga
79 Basin in order to reconstruct a detailed record of sea ice conditions for the early to late Holocene
80 in the northern Barents Sea (Fig. 1). The biomarker concentration data were presented
81 previously by Belt *et al.* (2015), but were not discussed in detail. In the current study, therefore,
82 we provide a more in-depth discussion of the individual and combined (i.e. PIP₂₅) biomarker
83 data, including, for the first time, semi-quantitative estimates of SpSIC based on the recent
84 calibration study by Smik *et al.* (2016). In addition, and similar to Werner *et al.* (2013, 2014),
85 planktic foraminiferal fauna assemblages and stable carbon and oxygen isotopes ($\delta^{18}\text{O}$, $\delta^{13}\text{C}$)
86 have also been measured to obtain a combined multiproxy record of sea ice conditions and sub-
87 surface water masses, thus demonstrating the interaction of sea ice and inflow of Atlantic Water.
88 The study site is located between the Atlantic Water characterized southern Barents Sea and
89 the central Arctic Ocean and is, therefore, influenced by Atlantic derived water masses
90 (Abrahamsen *et al.*, 2006) but also experiences seasonal sea ice conditions (Fig. 1). As such, it
91 represents a key location for reconstructing Holocene changes in sea ice conditions and Atlantic
92 Water inflow. Using our Holocene proxy data, we also propose different oceanographic
93 scenarios that emphasize the changing interactions between sea ice conditions and near-surface
94 waters and these are discussed further by comparing the proxy data with outcomes from
95 previous studies from the region.

96

97 *Sea ice biomarker background information*

98 Following the initial discovery of the Arctic sea ice proxy IP₂₅ (Belt *et al.*, 2007), analysis of
99 this biomarker has subsequently led to sea ice reconstructions for various sub-Arctic and Arctic
100 regions: the central Arctic Ocean (Xiao *et al.*, 2015a, 2015b), the Labrador Sea (Weckström *et*
101 *al.*, 2013), the Canadian Arctic (Vare *et al.*, 2009), the Bering Sea/North Pacific (Méheust *et*
102 *al.*, 2013, 2015), the Chukchi Sea (Polyak *et al.*, 2016; Stein *et al.*, 2016a), the East Siberian
103 Sea (Stein *et al.*, 2016a), the Laptev Sea (Fahl and Stein 2012; Xiao *et al.*, 2013), the Barents
104 Sea (Vare *et al.*, 2010; Berben *et al.*, 2014), the Fram Strait (Müller *et al.*, 2009, 2012; Cabedo-
105 Sanz *et al.*, 2013, 2016a; Knies *et al.*, 2014; Müller and Stein, 2014) and the
106 Greenland/Norwegian Seas (Massé *et al.*, 2008; Cabedo-Sanz *et al.*, 2016b). Furthermore, IP₂₅
107 appears stable within Arctic sediments to permit sea ice reconstructions over even longer
108 timescales (e.g. going back into the Pliocene (Knies *et al.*, 2014) and the Miocene (Stein *et al.*,
109 2016b). IP₂₅ is biosynthesized by certain Arctic sea ice diatoms and is thus usually found in
110 areas with seasonal sea ice conditions (e.g. Belt *et al.*, 2007; Brown *et al.*, 2011, 2014; Belt and
111 Müller, 2013). In order to provide complementary information regarding open water conditions,
112 Müller *et al.* (2009) proposed the additional measurement of phytoplankton biomarkers, such
113 as brassicasterol. In addition, by combining IP₂₅ and phytoplankton biomarker concentrations,
114 in the form of the so-called PIP₂₅ index, a method of elucidating semi-quantitative estimates of
115 sea ice conditions has been proposed (Müller *et al.*, 2011). However, application of the PIP₂₅
116 method is not always straightforward because some phytoplankton markers such as
117 brassicasterol may also have non-pelagic sources and their generally higher concentration
118 compared to IP₂₅ requires the use of a balance factor in the calculation of PIP₂₅, which can be
119 problematic (for a detailed discussion, see Belt and Müller, 2013; Navarro-Rodriguez *et al.*,
120 2013; Belt *et al.*, 2015; Xiao *et al.*, 2015a; Smik *et al.*, 2016). A recent study by Belt *et al.*
121 (2015), however, demonstrated that a further phytoplankton-derived HBI biomarker, more
122 specifically HBI III, was relatively abundant for locations within the marginal ice zone or close
123 to the winter ice margin in the Barents Sea, thus representing an alternative indicator of open
124 water conditions. In addition, since HBI III has a more constrained source (diatoms) and has
125 sedimentary concentrations much closer to those of IP₂₅, some of the problems associated with
126 using some other phytoplankton biomarkers can potentially be avoided. In a subsequent study,
127 Smik *et al.* (2016) also demonstrated that PIP₂₅ values based on IP₂₅ and HBI III could provide
128 realistic estimates of SpSIC for the Barents Sea, while a threshold value of 0.8 was suggested
129 as providing evidence for the presence of summer sea ice (>5% summer sea ice concentration
130 (SuSIC)).

132 **Study area and oceanographic setting**

133 The Barents Sea is an epicontinental shelf located between the Norwegian-Russian coast,
134 Novaya Zemlya and the Svalbard and Franz Josef Land archipelagos (Fig. 1). The northern
135 boundary of the Barents Sea is defined by the Nansen Basin continental slope (Jakobsson *et al.*,
136 2004). The Barents Sea is characterized by several water masses and represents a major passage
137 for Atlantic Water entering the Arctic Ocean (Carmack *et al.*, 2006; Rudels *et al.*, 2014).

138 The Norwegian Atlantic Current transports relatively warm and saline Atlantic Water towards
139 the high latitude North Atlantic Ocean (Hopkins, 1991) (Fig. 1a). Before entering the Barents
140 Sea, the Norwegian Atlantic Current splits into two different branches, the West Spitsbergen
141 Current and the North Cape Current, respectively (Fig. 1a). Both of these currents transport the
142 warm saline Atlantic Water into the Arctic Ocean (Rudels *et al.*, 2014). Within the Barents Sea,
143 Atlantic Water is entered from both the north and the southwest. The West Spitsbergen Current
144 flows northwards along the western Barents Sea slope and splits into three branches in the Fram
145 Strait; the Return Atlantic Current, the Yermak Branch and the Svalbard Branch (Fig. 1a) (e.g.
146 Manley, 1995). The latter enters the Arctic Ocean north of Svalbard as a sub-surface current
147 flowing eastward and beyond the Franz Victoria and St. Anna Troughs (Abrahamsen *et al.*,
148 2006; Rudels *et al.*, 2014). A sub-surface inflow of Atlantic Water derived from the Svalbard
149 Branch enters the Barents Sea via the Northern Barents Sea Opening (Fig. 1a). Subsequently,
150 Atlantic Water is advected south-westwards into the northern Barents Sea and has been
151 observed year-round in the Olga Basin (Abrahamsen *et al.*, 2006) where the studied sediment
152 core is located. Although the major sub-surface water mass in the Olga Basin is Atlantic Water
153 derived from the Svalbard Branch (Gammelsrød *et al.*, 2009; Klitgaard Kristensen *et al.*, 2013),
154 the area is furthermore influenced by Atlantic Water that enters as a submerged flow from the
155 south (e.g. Novitskiy, 1961; Loeng, 1991; Pfirman *et al.*, 1994; Aksenov *et al.*, 2010). The latter
156 is brought to the area by the North Cape Current flowing northwards via the Barents Sea
157 Opening into the southern Barents Sea, parallel to the coastal current system (Loeng, 1991;
158 Loeng *et al.*, 1993; Midttun, 1985; Rudels, 1987) (Fig. 1a). After mixing and heat loss, Atlantic
159 Water exits the Barents Sea via the Barents Sea Exit and reaches the Arctic Ocean via the St.
160 Anna Trough (e.g. Schauer *et al.*, 2002; Rudels *et al.*, 2014) (Fig. 1a).

161 In addition to relatively warm Atlantic Water, the Barents Sea is also influenced by Polar Water
162 that is brought from the Arctic Ocean into the Barents Sea through the Franz Victoria and St.

163 Anna Troughs, via the East Spitsbergen Current and the Bear Island Current, respectively
164 (Hopkins, 1991) (Fig. 1a). Arctic Water is formed when relatively warm Atlantic Water
165 converges and merges with cold, less saline and ice loaded Polar Water (Hopkins, 1991). Hence,
166 surface water in the north-eastern Barents Sea is, in contrast to the Atlantic Water dominated
167 south-western Barents Sea, dominated by Arctic Water characterized by reduced temperature
168 and salinity, as well as seasonal sea ice conditions (Hopkins, 1991). A CTD profile taken at the
169 core location illustrates the presence of Arctic Water at the surface, with Atlantic Water below
170 ca. 150 m (Fig. 1c; Table S1).

171 The oceanic fronts dividing these different water masses are one of the main oceanographic
172 features of the near-surface waters of the Barents Sea (Pfirman *et al.*, 1994). Defined as a sharp
173 climatic gradient in terms of temperature, salinity and sea ice conditions, the Polar and Arctic
174 fronts are the respective boundaries between Polar/Arctic and Arctic/Atlantic waters. The
175 positions of the Polar and Arctic fronts are closely related to the overall sea ice conditions and,
176 in particular, align with the average summer and winter sea ice margins, respectively (Vinje,
177 1977). Although sea ice advection from the Arctic Ocean does occur, sea ice within the Barents
178 Sea is mainly formed locally during autumn and winter (Loeng, 1991). The southward extent
179 of the oceanic fronts, and hence the sea ice conditions in particular, are regulated by the inflow
180 of Atlantic Water into the western Barents Sea, which controls the mainly ice-free Atlantic
181 domain in the south-western Barents Sea (Årthun *et al.*, 2012). In contrast, the north-eastern
182 Barents Sea experiences large changes in seasonal sea ice conditions (Vinje, 2001; Sorteberg
183 and Kvingedal, 2006) with maximum sea ice conditions during March/April and minimum
184 occurring throughout August/September (Fig. 1b). Annual sea ice variability during recent
185 decades might be explained by factors such as cyclone activity, which cause fluctuations in sea
186 ice transport, to and from the Arctic Ocean into the north-eastern Barents Sea (Kwok *et al.*,
187 2005; Sorteberg and Kvingedal, 2006; Ellingsen *et al.*, 2009; Kwok, 2009).

188 The interplay between water masses and other influences that impact sea ice formation in the
189 Barents Sea determine the position of the marginal ice zone, an area characterized by high
190 surface productivity during the summer season (e.g. Smith and Sakshaug, 1990). Within the
191 Barents Sea, enhanced primary production results from a peak algal bloom along the ice margin
192 during spring as sea ice retreats (Sakshaug *et al.*, 1992). In addition, the advection of Atlantic
193 Water contributes to longer productive seasons, compared to other Arctic areas (Wassmann,
194 2011). Consequently, the Barents Sea is one of the most productive areas of the Arctic Seas
195 (Wassmann *et al.*, 2006; Wassmann, 2011).

196

197 **Material and methods**

198 A 245 cm long marine sediment core NP05-11-70GC was retrieved in 2005 by the RV *Lance*
199 south of Kong Karls Land (Olga Basin) within the northern Barents Sea (78.40° N, 32.42° E;
200 293 m water depth) using a gravity coring device (Fig. 1). The upper section of the core (0–124
201 cm; 1-cm intervals) was investigated in the current study and was characterized by
202 homogeneous sediments rich in silty clay deposited in a marine environment.

203

204 *Chronology*

205 A depth-age model for NP05-11-70GC was developed using linear interpolation between three
206 calibrated AMS ¹⁴C dates obtained from mixed benthic foraminifera as described by Berben
207 (2014) and Belt *et al.* (2015) (Fig. 2; Table 1; Table S2). In order to try and improve the age
208 control, attempts to obtain more ¹⁴C dates were made by collecting all benthic foraminifera at
209 each core level selected for microfossil analyses (i.e. every cm). Unfortunately, additional ¹⁴C
210 measurements were prevented due to the very low numbers of foraminifera (and thus
211 insufficient amounts of CaCO₃ (Fig. 4)). Nonetheless, the lithological description of a marine
212 sediment core from a very nearby location in the northern Barents Sea also indicate a well-
213 defined homogeneous unit corresponding to Holocene sediments (Klitgaard Kristensen *et al.*,
214 2013). Thus, based on lithological similarities, together with some younger AMS ¹⁴C dates
215 (<2000 cal a BP) in a nearby core, the NP05-11-70GC core top is assumed to represent modern
216 age. The AMS ¹⁴C dates were calibrated using Calib 6.1.1 (Stuiver and Reimer, 1993) and the
217 Marine09 calibration curve (Reimer *et al.*, 2009). A local reservoir age (ΔR) of 105±24
218 suggested for the Svalbard area by Mangerud *et al.* (2006) was used in the calibration (Table
219 1).

220

221 *Biomarker analysis*

222 To reconstruct past sea ice conditions, the seasonal sea ice biomarker IP₂₅ and the open water
223 phytoplankton biomarkers (brassicasterol and HBI III) were analysed in 49 sub-samples (ca. 1
224 g taken from the same bulk sediment samples used for foraminiferal analysis). Prior to analysis,

225 sub-samples were freeze-dried and stored at -20 °C. The general methodology for biomarker
226 extraction, purification and analysis was as previously described by Belt *et al.* (2012) and
227 Brown and Belt (2012). Analytical reproducibility was monitored using a sediment with known
228 biomarker concentrations for every 10–12 extracted sediment samples (analytical error <6%,
229 n=5). Lipid quantification was conducted using the integrated peak areas of each biomarker and
230 the internal standard, an instrumental response factor, and the masses of the extracted sediment
231 and internal standard (Belt *et al.*, 2012). Biomarker concentrations, normalized to dry weight
232 sediment mass ($\mu\text{g/g sed.}$) as presented previously (Belt *et al.*, 2015), were further normalized
233 to total organic carbon ($\mu\text{g/g TOC}$) in order to compensate possible regional differences in
234 production and degradation in sediments (Belt and Müller, 2013). The weight percentages (wt.
235 %) of TOC (n=43) were determined using a Carlo Erba EA 1110 elemental analyzer at
236 Plymouth University. In order to remove any inorganic carbonate, ca. 100 mg of freeze-dried
237 sediment was digested in HCl (1mL; 18h).

238 To investigate past sea ice conditions more quantitatively, IP₂₅ and phytoplankton biomarkers
239 were used to calculate the so-called P_BIP₂₅ and P_{III}IP₂₅ indices (i.e. PIP₂₅ based on brassicasterol
240 and HBI III, respectively) (Müller *et al.*, 2011; Belt *et al.*, 2015). Calculation of the P_BIP₂₅ index
241 was achieved using Eq. 1, which includes a concentration balance factor (c ; Eq. 2) to
242 compensate for the significant concentration difference between IP₂₅ and brassicasterol (Müller
243 *et al.*, 2011).

$$244 \quad P_{BIP_{25}} = IP_{25} / (IP_{25} + (\text{brassicasterol} * c)) \quad [\text{Eq. 1}]$$

$$245 \quad c = \text{mean } IP_{25} / \text{mean brassicasterol} \quad [\text{Eq. 2}]$$

246 Calculation of P_{III}IP₂₅ indices was achieved by replacing brassicasterol concentrations (Eq. 1)
247 with those of HBI III. The balance factor, c , was calculated according to the relative mean
248 concentrations of IP₂₅ and HBI III (i.e. as per brassicasterol; Eq. 2) and we also used a value of
249 0.63, derived from a regional calibration of surface sediments from the Barents Sea (Belt *et al.*,
250 2015; Smik *et al.*, 2016). In practice, P_{III}IP₂₅ values using a c term based on Eq. 2 (0.84) were
251 very similar to those using the value of c derived from the surface sediment calibration (0.63;
252 Smik *et al.*, 2016). For simplicity, we present data using the surface sediment calibration only.
253 Semi-quantitative estimates of SpSIC were also made using the P_{III}IP₂₅ data and the calibration
254 of Smik *et al.* (2016) (Eq. 3) (for more background information, see Introduction).

$$255 \quad \text{SpSIC } (\%) = (P_{III}IP_{25} - 0.0692) / 0.0107 \quad [\text{Eq. 3}]$$

256

257 *Planktic foraminifera*

258 The sediment core was opened, and the sediments were sampled and frozen within 48 hours.
259 Sediment samples were freeze-dried, wet-sieved through three different size fractions (1000,
260 100 and 63 μm), and dried at 40 °C. Planktic foraminiferal assemblages were determined for
261 123 samples using the 100–1000 μm size fraction following Knudsen (1998). Following
262 Forcino (2012), the relative abundances (%) of each species were calculated for samples
263 containing more than 25 specimens (82 samples). Identification of *Neogloboquadrina*
264 *pachyderma* and *Neogloboquadrina incompta* species was achieved following Cifelli (1961)
265 and Darling *et al.* (2006), and planktic foraminiferal concentrations (#/g sed.) were calculated.

266 As the planktic foraminiferal assemblages might be affected by carbonate dissolution, it is
267 important to assess the impact of preservation changes on the planktic foraminiferal data (e.g.
268 Zamelczyk *et al.*, 2013). Here, the preservation conditions were investigated by analysing
269 preservation indicators such as the mean shell weight of *N. pachyderma* and the percentage of
270 fragmentation of planktic foraminiferal tests. A loss in the mean shell weight can be used to
271 identify dissolution in the water column and sediment surface (Broecker and Clark, 2001;
272 Barker and Elderfield, 2002; Barker *et al.*, 2004). Hence, 25 well preserved (visually) and
273 square shaped *N. pachyderma* specimens were picked from each sample from a narrow size
274 range (150–250 μm) in order to reduce problems of ontogeny and size difference induced
275 variability (Barker *et al.*, 2004). It was possible to obtain a mean shell weight (μg) of the 25
276 picked specimens per sample of *N. pachyderma* using a Mettler Toledo microbalance (0.1 μg
277 sensitivity; 110 samples). Further, the degree of fragmentation indicates the dissolution induced
278 weakening of the tests as well as dissolution processes within the sediment (Conan *et al.*, 2002).
279 The fragmentation (%) of planktic foraminiferal tests was calculated for the 82 samples that
280 contained a total number of >25 specimens within the 100–1000 μm size fraction. The
281 fragmentation was calculated using the equation proposed by Pfuhl and Shackleton (2004) (Eq.
282 4).

$$283 \text{ Fragmentation} = ((\# \text{fragments/g}) / ((\# \text{fragments/g}/3) + (\# \text{tests/g}))) * 10 \quad [\text{Eq. 4}]$$

284

285 *Stable carbon and oxygen isotope analysis*

286 The stable carbon and oxygen isotopic compositions of planktic foraminiferal shells ($\delta^{18}\text{O}$,
287 $\delta^{13}\text{C}$) are widely used to reflect the ambient sea water mass properties in which they have been
288 calcified. In particular, $\delta^{18}\text{O}$ is a proxy for temperature and salinity, whereas $\delta^{13}\text{C}$ variations
289 reflect primary production and stratification changes (e.g. Spielhagen and Erlenkeuser, 1994;
290 Katz *et al.*, 2010). The $\delta^{18}\text{O}$ and $\delta^{13}\text{C}$ analyses were performed on the foraminiferal tests of *N.*
291 *pachyderma*. All specimens were selected from a narrow size range (150–250 μm) in order to
292 minimize size dependent effects on isotopic composition (Aksu and Vilks, 1988; Keigwin and
293 Boyle, 1989; Oppo and Fairbanks, 1989; Donner and Wefer, 1994; Bauch *et al.*, 2000).
294 Sufficient amount of specimens were obtained from 105 samples. Samples were analysed using
295 a Finnigan MAT 253 mass spectrometer coupled to an automated Kiel IV Carbonate
296 Preparation Device at the Geological Mass Spectrometer (GMS) Laboratory at the University
297 of Bergen. These measurements were conducted with a reproducibility of ± 0.06 ‰ ($\delta^{18}\text{O}$) and
298 ± 0.03 ‰ ($\delta^{13}\text{C}$). Data are reported on the ‰ versus VPDB scale calibrated with NBS-19.
299 Corrections for the ice volume effect were applied on the measured $\delta^{18}\text{O}$ values according to
300 Fairbanks (1989). No vital effect corrections were applied for the isotope measurements in this
301 study as published estimates of species-specific vital effects are often inconsistent (e.g. Kohfeld
302 *et al.*, 1996; Bauch *et al.*, 1997; Stangeew, 2001; Simstich *et al.*, 2003), possibly due to seasonal
303 changes of the apparent vital effect (Jonkers *et al.*, 2010).

304

305 **Results**

306 The resulting depth-age model ranges between the present and ca. 9400 cal a BP (Fig. 2). The
307 depth-age model presented here has its limitations (for a detailed discussion, see Chronology)
308 and hence, for this reason, assigned ages should be taken with caution. Therefore, all data plots
309 presenting the results of this study also include a depth scale, although the results are described
310 with respect to age to enable us to place them into a wider context, both spatially and temporally,
311 when comparing them with previously published results. Despite the limitations of the age
312 control, which prevents the determination of centennial-scale changes, we believe it is
313 nonetheless feasible to describe the general early to late Holocene changes with some
314 confidence.

315

316 *Biomarker data*

317 The initial decrease in IP₂₅ concentrations (2 data points) followed by low values, coincides
318 with increased concentrations of both brassicasterol and HBI III ca. 9500–8500 cal a BP (Fig.
319 3a-c; Table S3). Hereafter, IP₂₅ concentrations show slightly higher values, whereas
320 brassicasterol and HBI III show decreased concentrations towards ca. 5900 cal a BP (Fig. 3a-
321 c). During this entire time interval (i.e. ca. 9500–5900 cal a BP), a decreasing trend in TOC is
322 also observed, although values remain relatively high (Fig. 3d; Table S3). From ca. 5900–2700
323 cal a BP, the concentration of IP₂₅ increases further, while brassicasterol and HBI III both
324 decrease although TOC values remain relatively stable (Fig. 3a-d). The last ca. 2700 cal a BP
325 are characterized by the highest concentrations of IP₂₅ and relatively low (but stable)
326 concentrations of brassicasterol and HBI III (Fig. 3a-c). Although the TOC values fluctuate
327 somewhat throughout this period, the absolute values are the lowest within the entire record
328 (Fig. 3d).

329 Both P_BIP₂₅ and P_{III}IP₂₅ indices, as well as the estimated SpSIC (which is linearly related to
330 P_{III}IP₂₅; Smik *et al.*, 2016), follow the same trends throughout the entire record (Fig. 3e-g; Table
331 S3). After the initial lowest values at ca. 9000 cal a BP, each of P_BIP₂₅, P_{III}IP₂₅ and SpSIC show
332 increasing (although still relatively low) values towards ca. 5900 cal a BP (Fig. 3e-g). The mean
333 SpSIC estimate ca. 9500–5900 cal a BP is ca. 25% (Fig. 3g). From ca. 5900–2700 cal a BP, the
334 P_BIP₂₅, P_{III}IP₂₅ and SpSIC records continue their increasing trend, albeit more gradually. The
335 estimated SpSIC shows a mean value of ca. 60% throughout this time interval (Fig. 3g) with
336 highest values towards ca. 2700 cal a BP. The P_BIP₂₅ reaches its highest value at the core top,
337 whereas the P_{III}IP₂₅ records a maximum value at ca. 1600 cal a BP after which it remains high
338 until the present (Fig. 3e-f). Estimates of SpSIC show a mean value of ca. 75% (Fig. 3g).
339 According to the threshold limit (P_{III}IP₂₅>0.8) suggested by Smik *et al.* (2016), the occurrence
340 of summer sea ice (SuSIC>5%) is estimated to have begun ca. 2700 cal a BP and remained a
341 consistent feature thereafter, until the present (Fig. 3f).

342

343 *Planktic foraminiferal preservation*

344 From ca. 9500–7300 cal a BP, the absolute abundances of planktic foraminifera remain
345 relatively low where after, they increase towards 5900 cal a BP (Fig. 4a; Table S4). From ca.
346 5900–2700 cal a BP, the planktic foraminiferal concentration has a broader range (Fig. 4a),
347 while in the last ca. 2700 cal a BP, three episodes of increased planktic foraminiferal

348 concentration values are observed ca. 2400–2000 cal a BP, ca. 1600–700 cal a BP, and ca. 400
349 cal a BP–present (Fig. 4a).

350 From ca. 9500–5900 cal a BP, the extent of fragmentation shows a mean value of 32%, whereas
351 the mean shell weight is highly variable until ca. 7300 cal a BP, followed by more stable values
352 (ca. 7.5 μg) towards ca. 5900 cal a BP (Fig. 4b-c; Table S4). The mean shell weight remains
353 relatively stable (ca. 7 μg) ca. 5900–2700 cal a BP, while the fragmentation record exhibits an
354 overall decrease (Fig. 4b-c). During the last ca. 2700 cal a BP, the degree of fragmentation
355 shows a small overall increase although there is mainly an increase in the amplitude (i.e. minima
356 and maxima between ca. 9–83%) (Fig. 4b). At the same time, the mean shell weight shows a
357 general decrease (Fig. 4c).

358

359 *Planktic foraminiferal fauna*

360 The planktic foraminiferal record is characterized by the presence of polar (*N. pachyderma*)
361 and sub-polar (*N. incompta*, *Turborotalita quinqueloba*, *Globigerinita glutinata*, *Globigerina*
362 *bulloides* and *Globigerinita. uvula*) species with *N. pachyderma* generally dominating the
363 assemblages (Fig. 4d-i; Table S4). From ca. 9500–7300 cal a BP, the fauna is dominated by *N.*
364 *pachyderma* (ca. 95%) followed by a period (ca. 7300–5900 cal a BP) with increased relative
365 abundances of *T. quinqueloba*, *N. incompta* and *G. glutinata* up to ca. 24, 27 and 4%,
366 respectively (Fig. 4d-g). After ca. 5900 cal a BP, the relative abundances of *T. quinqueloba* and
367 *N. incompta* decrease and remain relatively stable (ca. 3–4%) towards ca. 2700 cal a BP, while
368 *N. pachyderma* clearly dominates the planktic foraminiferal fauna (Fig. 4d-f). Throughout the
369 last ca. 2700 cal a BP, a reduction in *N. pachyderma* (towards ca. 65%) is accompanied by
370 increasing relative abundances of *G. glutinata* (ca. 5%) and *G. bulloides* (ca. 8%), whereas *T.*
371 *quinqueloba* and *N. incompta* reach their highest values between ca. 2400–2000 cal a BP, ca.
372 1600–700 cal a BP and ca. 400 cal a BP–present (Fig. 4d-h). The period from ca. 400 cal a BP–
373 present is characterized by a clear increase of *G. glutinata* (ca. 7%) and *G. bulloides* (ca. 6%),
374 in addition to a remarkable increase of *G. uvula* (ca. 7%) (Fig. 4g-i).

375

376 *Stable carbon and oxygen isotope data*

377 From ca. 9500–8800 cal a BP, the $\delta^{18}\text{O}$ (*N. pachyderma*) record has a mean value of 3.8 ‰
378 followed by a period (ca. 8800–7300 cal a BP) characterized by lighter values (Fig. 5a; Table
379 S5). A significant increase in $\delta^{18}\text{O}$ ca. 7600–7300 cal a BP is followed by heavier values that
380 fluctuate around ca. 3.7 ‰ until ca. 5900 cal a BP. The $\delta^{18}\text{O}$ record remains relatively stable
381 ca. 5900–2700 cal a BP with relatively heavy values (Fig. 5a). Throughout the last ca. 2700 cal
382 a BP, the $\delta^{18}\text{O}$ record shows decreased values in the range 3.5–4.0 ‰ (Fig. 5a).

383 The $\delta^{13}\text{C}$ record shows a decrease from 0.4 to 0.0 ‰ ca. 9500–8500 cal a BP (Fig. 5b; Table
384 S5). This trend is reversed at ca. 8500 cal a BP, with heavier $\delta^{13}\text{C}$ values towards ca. 5900 cal
385 a BP followed by an increase towards 0.9 ‰ ca. 5900–2700 cal a BP (Fig. 5b). The last ca.
386 2700 cal a BP are then characterized by a decreasing trend with $\delta^{13}\text{C}$ values in the range 0.3–
387 0.8 ‰ (Fig. 5b).

388

389 **Discussion**

390 Throughout the early to late Holocene, the palaeoceanographic record in NP05-11-70GC shows
391 an overall increase in sea ice reflecting the decline in solar insolation (Fig. 6a-d). Related IP25-
392 based reconstructions have been reported for other Arctic and sub-Arctic regions such as the
393 Fram Strait, the Laptev Sea, the East Siberian Sea and the Chukchi Sea (Stein *et al.*, 2016a), as
394 well as for the Canadian Arctic (Vare *et al.*, 2009; Belt *et al.*, 2010) and North Iceland (Cabedo-
395 Sanz *et al.*, 2016b). However, for some other regions, including the Alaskan margin (Polyak *et*
396 *al.*, 2016) and the western Barents Sea (Berben *et al.*, 2014), this long-term trend is not as
397 evident. The record presented here for the northern Barents Sea is described in terms of
398 individual time intervals reflecting the main stages of sea ice conditions and Atlantic Water
399 inflow. The intervals are: Period I (ca. 9500–5900 cal a BP), Period II (ca. 5900–2700 cal a BP)
400 and Period III (ca. 2700 cal a BP–present), although the interpretation of the timing of the exact
401 boundaries between these intervals should be considered with caution due to the limitations of
402 the age-depth model (see Chronology). Climate and oceanographic variations during these
403 periods are discussed and set into further context by comparison with previously published
404 records from the region.

405 Our interpretation of the sea ice conditions involves the identification of previously unavailable
406 semi-quantitative estimates of SpSIC and summer sea ice occurrence using a recently calibrated
407 biomarker approach, which has also permitted the proposal of different sea ice scenarios. To

408 obtain realistic representations for such sea ice conditions, known scenarios derived from
409 modern and historical observations of the Barents Sea (NSIDC) have been considered (Fig. 1b).
410 For example, the modern sea ice conditions have been derived from maximum (March) and
411 seasonal variability (April/August) in sea ice using satellite data obtained between 1981 and
412 2010 (NSIDC) (Fig. 7c). In terms of temporal changes, historical data from the Barents Sea
413 show variations in the mean sea ice margin position in April for four sub-periods between 1870
414 and 2002 (Divine and Dick, 2006). A north-easterly retreat of the sea ice margin since the
415 second half of the 19th century occurred after a significant cooling in the second half of the 18th
416 century (Divine and Dick, 2006) (Fig. 1b). This historical data from the Barents Sea illustrates
417 that the decadal migration pattern of the sea ice margins associated with climatic conditions can
418 reflect observed sea ice changes on an annual and/or seasonal time scale. Therefore, this key
419 dataset provides precedent for the proposed sea ice scenarios (and changes to these) within the
420 Barents Sea during the early to late Holocene.

421 With respect to the planktic foraminiferal preservation conditions, the proxy data is interpreted
422 as follows. Better calcium carbonate preservation has been associated with increased
423 production of organic matter in regions impacted by Atlantic Water (e.g. Hebbeln *et al.* 1998;
424 Henrich *et al.* 2002). In particular, for areas with enhanced Atlantic Water inflow towards the
425 Fram Strait, ocean currents appear to have a positive influence on the preservation of organic
426 matter in sediments (Birgel and Stein, 2004; Birgel *et al.*, 2004). The wide range in both
427 fragmentation and mean shell weight could therefore reflect variable environmental control,
428 preservation conditions or a combination of both. The high mean shell weight ca. 7300–5900
429 cal a BP indicates better preservation conditions, possibly related to an increased influence of
430 Atlantic Water (Fig. 4c). In contrast, throughout the last ca. 2700 cal a BP, the preservation
431 indicators (i.e. low mean shell weight and highly fluctuating fragmentation) show an overall
432 change towards enhanced dissolution (Fig. 4b-c). This may be caused by an increased influence
433 of sea ice formation and brine rejection which may form corrosive bottom water masses causing
434 dissolution at the sea floor (e.g. Midttun 1985; Steinsund and Hald 1994). Further, the low
435 planktic foraminiferal concentrations may seem to indicate poor preservation conditions,
436 however studies of recent planktic foraminifera show that low planktic foraminiferal
437 concentrations can be found within environments characterized by sea ice conditions (Carstens
438 *et al.* 1997; Pados and Spielhagen 2014). In addition, the data in this study is consistent with
439 planktic foraminiferal concentrations from the Barents Sea region (e.g. Klitgaard Kristensen *et*
440 *al.* 2013; Duplessy *et al.* 2001). When compared with other studies from the region (e.g.

441 Zamelczyk *et al.* 2012, 2013; Berben *et al.* 2014), however, the current fragmentation and mean
442 shell weight data indicate good preservation, especially throughout the early part of the record.
443 Therefore, the generally low planktic foraminiferal concentrations are attributed here to the
444 environmental conditions such as the shallow shelf environment influenced by Arctic Water
445 with a reduced salinity and the proximity of the sea ice margin.

446 Regarding the planktic foraminiferal oxygen isotope signal, studies of recent foraminiferal
447 calcite and the isotopic composition of water masses by Lubinski *et al.* (2001) demonstrate that,
448 in the Barents Sea, these are controlled mainly by temperature changes rather than salinity.
449 However, the water masses in the region are also influenced by meltwater and reduced
450 salinities, especially during the earliest part of the Holocene, although this influence probably
451 diminished around ca. 11 000 cal a BP (Klitgaard Kristensen *et al.*, 2013). Therefore, it is
452 further assumed that the stable isotope record has been mainly controlled by temperature.

453

454 *Period I (ca. 9500–5900 cal a BP): minimum sea ice conditions with reduced*
455 *SpSIC (ca. 25%)*

456 During Period I, low IP₂₅ concentrations reflect reduced seasonal sea ice, while high
457 brassicasterol and HBI III concentrations are indicative of open water and sea ice margin
458 conditions, respectively (Fig. 3a-c). At the same time, the lowest P_BIP₂₅ and P_{III}IP₂₅ values
459 indicate reduced spring sea ice conditions, with longer (warmer) summers suitable for
460 phytoplankton production (Müller *et al.*, 2011; Belt *et al.*, 2015; Smik *et al.*, 2016) (Fig. 3e-f),
461 which is also reflected by the generally higher TOC values (Fig. 3d). Maximum HBI III
462 concentrations indicate decreasing winter ice margin conditions from ca. 9500–8500 cal a BP
463 (Belt *et al.*, 2015), with SpSIC estimates consistently less than 50% (mean ca. 25%) (Fig. 3g)
464 and an absence of summer sea ice (Fig. 3f-g). The occurrence of reduced SpSIC and longer
465 (ice-free) summers is consistent with longer ice-free seasons and a retreated ice margin
466 observed in the northern Barents Sea (Duplessy *et al.*, 2001) and increased phytoplankton
467 production in the northern Fram Strait (Müller *et al.*, 2009, 2012) (for location of these study
468 sites please refer to Fig. 1). Reduced spring sea ice conditions likely indicate the occurrence of
469 the Holocene Thermal Maximum as recorded at the sea surface ca. 9300–6500 cal a BP. The
470 subsequent increase in IP₂₅ concentration after ca. 6500 cal a BP reflects a general enhancement
471 in sea ice conditions probably marking the gradual transition of the Holocene Thermal
472 Maximum towards Neoglacial conditions (Fig. 6b). Similar conclusions regarding timing and

473 termination of the Holocene Thermal Maximum based on IP₂₅ records have been made for the
474 Fram Strait (until ca. 8400 cal a BP; (Müller *et al.*, 2009)) and the West Svalbard margin, where
475 the last phase of the Holocene Thermal Maximum was recorded ca. 8500–7000 cal a BP (Müller
476 *et al.*, 2012). Furthermore, the observed disappearance of sea ice in the western Barents Sea
477 from ca. 10 700–7700 cal a BP has been linked previously to the Holocene Thermal Maximum
478 (Sarnthein *et al.*, 2003).

479 The light $\delta^{18}\text{O}$ (*N. pachyderma*) values ca. 8800–7300 cal a BP indicate a small temperature
480 rise, possibly reflecting a gradual shift towards a warmer sub-surface water mass due to
481 increased Atlantic Water inflow (Fig. 6e). The relatively light $\delta^{18}\text{O}$ values also coincide with
482 high insolation, thereby reflecting the Holocene Thermal Maximum at the core site (Fig. 6e).
483 The strong increase in $\delta^{18}\text{O}$ values ca. 7600–7300 cal a BP probably reflects its termination, a
484 conclusion consistent with observations of Duplessy *et al.* (2001) for a nearby location.
485 Furthermore, Hald *et al.* (2007) presented a time-transgressive Atlantic Water inflow from
486 south to north along the Norwegian and Svalbard margins. Risebrobakken *et al.* (2011)
487 suggested that this time-transgressive northward intensified heat advection resulted from major
488 reorganization of the ocean circulation following the deglaciation. Hence, throughout the
489 Holocene Thermal Maximum, high latitude radiative forcing was not responsible for the overall
490 conditions of the water column and ocean dynamics, although it might have further enhanced
491 the transport of warm salty water (Risebrobakken *et al.*, 2011). Within the broader study area,
492 Lubinski *et al.* (2001) associated decreasing $\delta^{18}\text{O}$ values ca. 10 000–6800 cal a BP with a
493 possible increase of surface water temperatures due to a return inflow of warm water. A stronger
494 Atlantic Water inflow delivered by the Svalbard Branch has also been recorded at the western
495 and northern Svalbard margins ca. 8000 cal a BP (Slubowska *et al.*, 2005; Werner *et al.*, 2013)
496 and in the Franz Victoria Trough ca. 7500 cal a BP (Duplessy *et al.*, 2001). However, since the
497 $\delta^{18}\text{O}$ values do not correspond to the observed time-transgressive pattern of the Svalbard
498 Branch, it is assumed that the core site was influenced by Atlantic Water inflow entering the
499 Barents Sea via the North Cape Current. This is consistent with decreased $\delta^{18}\text{O}$ observations in
500 the southern Barents Sea ca. 11 000–9800 cal a BP (Risebrobakken *et al.*, 2010), the western
501 Barents Sea ca. 10 000 cal a BP (Berben *et al.*, 2014) and the north-western Barents Sea ca.
502 7000 cal a BP (Klitgaard Kristensen *et al.*, 2013) (for study locations please refer to Fig. 1).

503 During Period I, the overall high relative abundances of *N. pachyderma*, in particular ca. 9500–
504 7300 cal a BP, suggest a dominance of Arctic Water masses and cold conditions at the study
505 site (Volkman, 2000). However, from ca. 7300–5900 cal a BP, the increased abundances of

506 sub-polar species as well as of total planktic foraminifera indicate a pronounced influence of
507 relatively warm Atlantic Water inflow at the core site (Bé and Tolderlund, 1971; Johannessen
508 *et al.*, 1994; Carstens *et al.*, 1997) (Fig. 6f-g). Correspondingly, elevated planktic foraminiferal
509 concentrations were recorded in the north-eastern Barents Sea and linked to an intrusion of
510 Atlantic Water (Duplessy *et al.*, 2001). Similar interpretations were made for the northern
511 Barents Sea (Klitgaard Kristensen *et al.*, 2013) and the western Barents Sea (Sarnthein *et al.*,
512 2003; Berben *et al.*, 2014).

513 Nonetheless, the timing of changes in Atlantic Water inflow based on planktic foraminiferal
514 assemblages (ca. 7300–5900 cal a BP) differs from that based on $\delta^{18}\text{O}$ (ca. 8800–7300 cal a
515 BP). In the Arctic Ocean, the calcification of *N. pachyderma* is linked to phytoplankton blooms
516 occurring mainly in August (Kohfeld *et al.*, 1996; Volkman, 2000), whereas the planktic
517 foraminiferal fauna reflects an annual signal. Additionally, sea ice conditions can result in a
518 shift in the growing season (e.g. Farmer *et al.*, 2008) and a species-specific change in its
519 calcification depth. Therefore, the $\delta^{18}\text{O}$ of *N. pachyderma* reflects a different temperature
520 compared to the total foraminiferal assemblage (Simstich *et al.*, 2003) and might reflect a
521 different signal with respect to seasonality and/or water depth. Furthermore, the faunal response
522 depends on more factors than temperature and salinity. For example, *T. quinqueloba* also
523 depends on the available food supply (e.g. Volkman, 2000) and is characteristic of Arctic Front
524 conditions in the western Barents Sea (Burhol, 1994). An increased nutrition availability
525 associated with oceanic front conditions might have followed later in time. Indeed, such a delay
526 in food supply is suggested by increasing $\delta^{13}\text{C}$ values ca. 7300–5800 cal a BP which likely
527 reflect enhanced primary production, possibly associated with increased seasonal sea ice
528 conditions, as suggested from the IP₂₅ data. Hence, the timing of increased relative abundances
529 of sub-polar species is probably related to a combination of enhanced Atlantic Water inflow
530 and increased nutrition availability, as seen previously in the northern Barents Sea (Duplessy
531 *et al.*, 2001).

532 For Period I, the new proxy data, combined with outcomes from previous studies, indicate that
533 the study site was characterized by reduced sea ice conditions during relatively short spring
534 seasons, enhanced phytoplankton production within the proximity of the sea ice margin, and a
535 winter sea ice margin in the proximity of the core site at ca. 78° N (Fig. 7a). These sea surface
536 conditions were likely influenced by maximum insolation, while the sub-surface water masses
537 were probably controlled more by oceanic dynamics (Andersson *et al.*, 2010; Risebrobakken *et*
538 *al.*, 2011). In particular, a time-transgressive Atlantic Water inflow resulted in initially cold

539 water masses followed by warmer Atlantic Water at the study site. The strengthening of
540 Atlantic Water inflow might have additionally contributed to the reduced sea ice conditions as
541 seen during modern times in the Barents Sea (Årthun *et al.*, 2012). Such a proposed sea ice
542 scenario implies that water masses south of the study area were ice free, consistent with open
543 water conditions observed in the western Barents Sea (Sarnthein *et al.*, 2003; Berben *et al.*,
544 2014) and the West Svalbard margin (Müller *et al.*, 2012) (Fig. 7a) during the early Holocene.

545

546 *Period II (ca. 5900–2700 cal a BP): marginal ice zone conditions with increasing*
547 *SpSIC (ca. 60%)*

548 Throughout Period II, higher IP₂₅ concentrations and parallel decreases in brassicasterol and
549 HBI III concentrations reflect increased seasonal sea ice with less open water conditions (Fig.
550 3a-c). Increasing P_BIP₂₅ and P_{III}IP₂₅ values indicate marginal ice zone conditions at the study
551 site (Müller *et al.*, 2011; Belt *et al.*, 2015) (Fig. 3e-f) with a mean SpSIC of ca. 60% but
552 increasing throughout this interval to ca. 70% (Fig. 6d). Despite a general increase in SpSIC,
553 however, the P_{III}IP₂₅ data suggest that the site was probably ice free throughout the summer
554 months (Smik *et al.*, 2016) (Fig. 6c). Similar IP₂₅-based reconstructions of sea ice conditions
555 have been attributed to mid Holocene Neoglacial cooling for the northern Fram Strait (Müller
556 *et al.*, 2009) and the West Svalbard margin (Müller *et al.*, 2012).

557 The heavy $\delta^{18}\text{O}$ (*N. pachyderma*) values during Period II indicate lower temperatures and a
558 decreased influence of Atlantic Water (Fig. 6e), consistent with previous observations from the
559 region (Duplessy *et al.*, 2001; Klitgaard Kristensen *et al.*, 2013). It has also been suggested that
560 Arctic Water from the north-eastern Barents Sea might have influenced the western Barents
561 Sea due to less heat advection from the south (Hald *et al.*, 2007).

562 The dominance of *N. pachyderma*, along with decreased abundances of sub-polar foraminifera,
563 such as *T. quinqueloba* and *N. incompta* indicate the prevailing presence of colder Arctic Water
564 at the core site (Volkman, 2000) (Fig. 6f-g). This is consistent with foraminifera-based
565 observations of cold conditions after ca. 5200 cal a BP in the eastern Fram Strait (Werner *et al.*,
566 2013) and reduced Atlantic Water inflow in the western Barents Sea (Sarnthein *et al.*, 2003).

567 Combined, the biomarker and microfossil proxy data indicate a continuous cooling trend during
568 Period II with a dominance of cold Arctic Water and an accompanying increase in SpSIC, likely

569 as a result of decreasing summer insolation and a cooler surface water layer. Consequently, the
570 strongly reduced Atlantic Water inflow could not have affected the sea ice conditions in the
571 same way as was proposed for Period I. In addition, our data suggest that the maximum winter
572 sea ice margin was probably located ca. 76–77° N or, at least, further south compared to the
573 Period I (Fig. 7a-b). This is in good agreement with sea ice conditions at the continental slope
574 of western Svalbard (Müller *et al.*, 2012), although sea ice did not extend as far as the western
575 Barents Sea (Berben *et al.*, 2014) (Fig. 7b). With respect to the position of the summer sea ice
576 margin, the increased P_{III}IP₂₅ values also suggest a location further south compared to Period I,
577 consistent with previous observations in the northern Barents Sea after ca. 6000 cal a BP
578 (Duplessy *et al.*, 2001; Klitgaard Kristensen *et al.*, 2013) (Fig. 7b).

579

580 *Period III (ca. 2700 cal a BP–present): Arctic frontal conditions with high SpSIC*
581 *(ca. 75%) and summer sea ice*

582 Increases to IP₂₅, P_BIP₂₅ and P_{III}IP₂₅ reflect further increases in spring sea ice conditions during
583 Period III (Fig. 3a; e-f), while lower brassicasterol and HBI III concentrations indicate less open
584 water phytoplankton production consistent with lower TOC values (Fig. 3b-d). These results
585 point to Arctic frontal conditions that are similar to the modern setting (Müller *et al.*, 2011; Belt
586 *et al.*, 2015). Indeed, the P_{III}IP₂₅-based SpSIC estimates (ca. 75%) align closely with
587 contemporary values derived from satellite records (Smik *et al.*, 2016) (Fig. 6c-d), while P_{III}IP₂₅
588 values generally >0.8 are also indicative of the occurrence of summer sea ice (Smik *et al.*,
589 2016), also a feature of the modern setting. Consistent with these findings, extended sea ice
590 conditions have been reported for the Fram Strait for the last ca. 3000 cal a BP (Müller *et al.*,
591 2012).

592 The mainly light, but variable, $\delta^{18}\text{O}$ (*N. pachyderma*) values, are most likely indicative of a
593 generally increased influence of Atlantic Water inflow (Fig. 6e), consistent with previous
594 reports of episodic increases in Atlantic Water for the northern Barents Sea (Duplessy *et al.*,
595 2001; Lubinski *et al.*, 2001), the western Barents Sea (Wilson *et al.*, 2011; Berben *et al.*, 2014)
596 and the Svalbard margin (Jernas *et al.*, 2013; Werner *et al.*, 2013) during the late Holocene.

597 The decrease in *N. pachyderma* and increased relative abundance of sub-polar foraminifera,
598 especially *G. bulloides*, which is usually associated with the warmest parts of the Norwegian
599 Atlantic Current (Johannessen *et al.*, 1994) also reflect the generally increasing influence of

600 Atlantic Water during this period (Fig. 6f-g). However, the fluctuations in the faunal data
601 throughout Period III still indicate variability in the influence of Atlantic Water consistent with
602 previous findings from the western Barents Sea (Sarnthein *et al.*, 2003).

603 The increase in sea ice conditions reflects an overall cooling trend recorded previously in
604 various Arctic terrestrial (e.g. Bjune *et al.*, 2009; Kaufman *et al.*, 2009), ice core (e.g. Kaufman
605 *et al.*, 2009; Divine *et al.*, 2011) and marine records (e.g. Slubowska *et al.*, 2005; Skirbekk *et*
606 *al.*, 2010), likely resulting from lower insolation affecting the sea surface. A negative solar
607 irradiance anomaly ca. 2850–2600 cal a BP may also have resulted in decreased ventilation of
608 the sub-surface waters, as corroborated by modelling experiments (Renssen *et al.*, 2006).
609 Meanwhile, the increased influence of Atlantic Water inflow might be attributed to stronger
610 stratification among the upper layers as seen in previous studies of the Barents Sea (Lubinski
611 *et al.*, 2001; Duplessy *et al.*, 2005; Risebrobakken *et al.*, 2010; Wilson *et al.*, 2011) and the
612 Svalbard margin (Jernas *et al.*, 2013; Werner *et al.*, 2013).

613 The occurrence of sea surface cooling and sub-surface warming indicates that Period III was
614 most likely characterized by a strong vertical stratification and a decoupling between the
615 atmosphere and the oceanic sub-surface. Summer insolation was at its lowest during Period III
616 (Fig. 6a), resulting in cooler atmospheric temperatures and potentially enhanced sea ice
617 production and/or reduced sea ice melt. In addition to the stronger vertical stratification of the
618 water column, the increased sea ice conditions probably also limited the heat exchange between
619 the atmosphere and the sub-surface water masses. In terms of seasonality, we suggest that
620 relatively long spring seasons with extensive sea ice conditions would have been accompanied
621 by shorter (and probably cooler) summers with lower phytoplankton production (Fig. 7c).
622 Overall, the site was characterized by extensive sea ice conditions (SpSIC typically ca. 75%)
623 with at least partial sea ice occurrence in the summer months (Fig. 7c). Such interpretations are
624 also consistent with previous qualitative reports of intensified sea ice occurrence in the northern
625 Barents Sea (Duplessy *et al.*, 2001; Klitgaard Kristensen *et al.*, 2013), increasing sea ice
626 conditions in the Fram Strait (Müller *et al.*, 2009, 2012; Werner *et al.*, 2014) and in the western
627 Barents Sea throughout the last ca. 1100 cal a BP (Berben *et al.*, 2014). Hence, the data suggest
628 a south-westwards transgression of the sea ice margin (Fig. 7c). Finally, the sea ice conditions
629 most likely exceeded the modern sea ice margin during the (pre-industrial) late Holocene (Fig.
630 7c). A slight reversal in the extent of spring sea ice conditions during recent decades and a
631 return to more open water conditions during summer (c.f. Period II) is evident during the last
632 ca. 100 yr from observational records (Divine and Dick, 2006).

633

634 **Conclusions**

635 Early to late Holocene semi-quantitative estimates of SpSIC and the qualitative occurrence of
636 summer sea ice in the northern Barents Sea have been reconstructed based on the variability of
637 source-specific biomarkers within a marine sediment core taken from the Olga Basin.
638 Additional proxy data based on planktic foraminifera that reflect the sub-surface water masses
639 have demonstrated the evolution of Atlantic Water inflow to the Barents Sea. The major
640 palaeoceanographic evolution can be summarised as follows: During Period I (ca. 9500–5900
641 cal a BP), reduced SpSIC (ca. 25%) was controlled, primarily, by relatively high summer
642 insolation. The core site was also influenced by Atlantic Water entering the Barents Sea via the
643 North Cape Current which caused an increased heat exchange between the ocean and the
644 atmosphere and likely contributed to reduced sea ice conditions. The site was probably located
645 close to the maximum winter sea ice margin, such that it experienced only relatively short
646 periods of sea ice during the spring together with long (ice-free) productive summers.

647 An overall cooling trend characterized Period II (ca. 5900–2700 cal a BP), with increased
648 SpSIC (ca. 60%) and delivery of cold Arctic Water. This interval was also characterized by a
649 general southward advance of the winter and summer sea ice margins, although, summer
650 months were still ice free.

651 Period III (ca. 2700 cal a BP–present) was marked by extensive SpSIC (ca. 75%), partial
652 summer sea ice occurrence and increased Atlantic Water inflow. Increased sea ice conditions
653 were probably induced by progressively lower insolation, while sub-surface warming due to
654 increased Atlantic Water demonstrates a likely decoupling between the atmosphere and the
655 ocean. The maximum winter sea ice margin was probably at its most southerly location within
656 the record, with long spring seasons of extensive sea ice conditions followed by shorter and less
657 productive summers. A slight retreat in the position of the winter sea ice margin is proposed for
658 recent decades based on observational records.

659

660 **Supporting information**

661 Additional supporting information related to this article may be found in the online version of
662 this article.

663 **Table S1.** CTD data presented in Fig. 1

664 **Table S2.** Age model presented in Fig. 2

665 **Table S3.** Biomarker data presented in Fig. 3

666 **Table S4.** Foraminiferal fauna data presented in Fig. 4

667 **Table S5.** Stable isotope data presented in Fig. 5

668

669 *Acknowledgements.* All data used in this work can be found in the supporting information for this paper. This work
670 was carried out within the framework of the Initial Training Network program “Changing Arctic and Subarctic
671 Environments” (CASE, Grant Agreement No. 238111) funded by the European Commission within the 7th
672 Framework Program People, the Research Council of Norway in addition to UiT–The Arctic University of Norway
673 and the Norwegian Polar Institute. Steffen Aagaard-Sørensen received financial support from the GlaciBar
674 (Glaciations in the Barents Sea area) project funded by the Norwegian Research Council (NRC grant 200672/S60),
675 Statoil, Det Norske and BG Norge. Thanks are also extended to Trine Dahl and Julia Sen for assisting with
676 laboratory work in addition to Patricia Cabedo-Sanz for valuable discussions. Finally, we thank Ruediger Stein
677 and one anonymous reviewer for their constructive feedback improving this manuscript.

678

679 **References**

- 680 Abrahamsen E, Østerhus S, Gammelsrød T. 2006. Ice draft and current measurements from the
681 north-western Barents Sea, 1993-96. *Polar Research* **25**: 25-37.
- 682 Aksenov Y, Bacon S, Coward AC, Nurser AJG. 2010. The North Atlantic inflow to the Arctic
683 Ocean: high-resolution model study. *Journal of Marine Systems* **79**: 1-22.
- 684 Aksu AE, Vilks G. 1988. Stable isotopes in planktonic and benthic foraminifera from Arctic
685 Ocean surface sediments. *Canadian Journal of Earth Sciences* **25**: 701-709.
- 686 Andersson C, Pausata FSR, Jansen E, Risebrobakken B, Telford RJ. 2010. Holocene trends in
687 the foraminifer record from the Norwegian Sea and the North Atlantic Ocean. *Climate of the*
688 *Past* **6**: 179-193.
- 689 Barker S, Elderfield H. 2002. Foraminiferal calcification response to glacial interglacial
690 changes in atmospheric CO₂. *Science* **297**: 883-836.
- 691 Barker S, Kiefer T, Elderfield H. 2004. Temporal changes in North Atlantic circulation
692 constrained by planktonic foraminiferal shell weights. *Paleoceanography* **19**: PA3008.
- 693 Bauch D, Carstens J, Wefer G. 1997. Oxygen isotope composition of living *Neogloboquadrina*
694 *pachyderma* (sin.) in the Arctic Ocean. *Earth and Planetary Science Letters* **146**: 47-58.
- 695 Bauch D, Carstens J, Wefer G, Thiede J. 2000. The imprint of anthropogenic CO₂ in the Arctic
696 Ocean: evidence from planktic δ¹³C data from water column and sediment surfaces. *Deep-Sea*
697 *Research Pt. II* **9-11**: 1791-1808.
- 698 Bé AWH, Tolderlund DS. 1971. Distribution and ecology of living planktonic foraminifera in
699 surface waters of the Atlantic and Indian Oceans. In *The micropaleontology of oceans*, Funnel
700 BM, Riedel WR (eds). Cambridge University Press: London; 105-149.
- 701 Belt ST, Massé G, Rowland SJ, Poulin M, Michel C, LeBlanc B. 2007. A novel chemical fossil
702 of palaeo sea ice: IP₂₅. *Organic Geochemistry* **38**: 16-27.
- 703 Belt ST, Vare LL, Massé G, Manners HR, Price JC, MacLachlan SE, Andrews JT, Schmidt S.
704 2010. Striking similarities in temporal changes to spring sea ice occurrence across the central
705 Canadian Arctic Archipelago over the last 7000 years. *Quaternary Science Reviews* **29**: 3489-
706 3504.
- 707 Belt ST, Brown TA, Navarro Rodriguez A, Cabedo Sanz P, Tonkin A, Ingle R. 2012. A
708 reproducible method for the extraction, identification and quantification of the Arctic sea ice
709 proxy IP₂₅ from marine sediments. *Analytical Methods* **4**: 705-713.
- 710 Belt ST, Müller J. 2013. The Arctic sea ice biomarker IP₂₅: a review of current understanding,
711 recommendations for future research and applications in palaeo sea ice reconstructions.
712 *Quaternary Science Reviews* **79**: 9-25.
- 713 Belt ST, Cabedo-Sanz P, Smik L, Navarro-Rodriguez A, Berben SMP, Knies J, Husum K. 2015.
714 Identification of paleo Arctic winter sea ice limits and the marginal ice zone: Optimised
715 biomarker-based reconstructions of late Quaternary Arctic sea ice. *Earth and Planetary Science*
716 *Letters* **431**: 127-139.

717 Berben SMP. 2014. *A Holocene palaeoceanographic multi-proxy study on the variability of*
718 *Atlantic water inflow and sea ice distribution along the pathway of Atlantic water*. The Arctic
719 University of Norway (PhD thesis).

720 Berben SMP, Husum K, Cabedo-Sanz P, Belt ST. 2014. Holocene sub-centennial evolution of
721 Atlantic water inflow and sea ice distribution in the western Barents Sea. *Climate of the Past*
722 **10**: 181-198.

723 Berger A. 1978. Long-term variations of daily insolation and quaternary climatic changes.
724 *Journal of Atmospheric Sciences* **35**: 2363-2367.

725 Birgel D, Stein R. 2004. Northern Fram Strait and Yermak Plateau: Distribution, variability and
726 burial of organic carbon and paleoenvironmental implications. In *The organic carbon cycle in*
727 *the Arctic Ocean*, Stein R, Macdonald RW (eds). Springer-Verlag: Berlin; 279-295.

728 Birgel D, Stein R, Hefter J. 2004. Aliphatic lipids in recent sediments of the Fram Strait/Yermak
729 Plateau (Arctic Ocean): composition, sources and transport processes. *Marine Chemistry* **88**:
730 127-160.

731 Bjune AE, Seppä H, Birks HJB. 2009. Quantitative summer temperature reconstructions for the
732 last 2000 years based on pollen-stratigraphical data from northern Fennoscandia. *Journal of*
733 *Paleolimnology* **41**: 43-56.

734 Broecker WS, Clark E. 2001. An evaluation of Lohmann's foraminifera weight dissolution
735 index. *Paleoceanography* **16**: 531-534.

736 Brown TA, Belt ST, Philippe B, Mundy CJ, Massé G, Poulin M, Gosselin M. 2011. Temporal
737 and vertical variations of lipid biomarkers during a bottom ice diatom bloom in the Canadian
738 Beaufort Sea: Further evidence for the use of the IP₂₅ biomarker as a proxy for spring Arctic
739 sea ice. *Polar Biology* **34**: 1857-1868.

740 Brown TA, Belt ST. 2012. Identification of the sea ice diatom biomarker IP₂₅ in Arctic benthic
741 macrofauna: Direct evidence for a sea ice diatom diet in Arctic heterotrophs. *Polar Biology* **35**:
742 131-137.

743 Brown TA, Belt ST, Tatarek A, Mundy CJ. 2014. Source identification of the Arctic sea ice
744 proxy IP₂₅. *Nature Communications* **5**: 4197.

745 Burhol ALS. 1994. *Recent distribution of planktonic foraminifera on the Svalbard-Barents*
746 *margin*. University of Tromsø (Master thesis).

747 Cabedo-Sanz P, Belt ST, Knies J, Husum K. 2013. Identification of contrasting seasonal sea
748 ice conditions during the Younger Dryas. *Quaternary Science Reviews* **79**: 74-86.

749 Cabedo-Sanz P, Belt ST. 2016a. Seasonal sea ice variability in eastern Fram Strait over the last
750 2000 years. *Arktos* **2(22)**: 1-12.

751 Cabedo-Sanz P, Belt ST, Jennings AE, Andrews JT, Geirsdóttir Á. 2016b. Variability in drift
752 ice export from the Arctic Ocean to the North Icelandic Shelf over the last 8,000 years: a multi
753 proxy evaluation. *Quaternary Science Reviews* **146**: 99-115.

754 Carmack E, Barber D, Christensen J, Macdonald R, Rudels B, Sakshaug E. 2006. Climate
755 variability and physical forcing of the food webs and the carbon budget on panarctic shelves.
756 *Progress in Oceanography* **71**: 145-181.

- 757 Carstens J, Hebbeln D, Wefer G. 1997. Distribution of planktic foraminifera at the ice margin
758 in the Arctic (Fram Strait). *Marine Micropaleontology* **29**: 257-269.
- 759 Cifelli R. 1961. *Globigerina incompta*, a new species of pelagic foraminifera from the North
760 Atlantic. *Contributions Cushman Foundation Foraminiferal Research* **12**: 83-86.
- 761 Conan SMH, Ivanova EM, Brummer G-JA. 2002. Quantifying carbonate dissolution and
762 calibration of foraminiferal dissolution indices in the Somali Basin. *Marine Geology* **182**: 325-
763 349.
- 764 Darling KF, Kucera M, Kroon D, Wade CM. 2006. A resolution for the coiling direction
765 paradox in *Neogloboquadrina pachyderma*. *Paleoceanography* **21**: PA2011.
- 766 Divine DV, Dick C. 2006. Historical variability of sea ice edge position in the Nordic Seas.
767 *Journal Geophysical Research* **111**: C01001.
- 768 Divine D, Isaksson E, Martma T, Meijer HAJ, Moore J, Pohjola V, van de Wal RSW,
769 Godtliobsen F. 2011. Thousand years of winter surface air temperature variations in Svalbard
770 and northern Norway reconstructed from ice-core data. *Polar Research* **30**: 7379.
- 771 Donner B, Wefer G. 1994. Flux and stable isotope composition of *Neogloboquadrina*
772 *pachyderma* and other planktonic foraminifers in the Southern Ocean (Atlantic sector). *Deep-*
773 *Sea Research Pt. I* **41**: 1733-1743.
- 774 Duplessy JC, Ivanova E, Murdmaa I, Paterne M, Labeyrie L. 2001. Holocene paleoceanography
775 of the northern Barents Sea and variations of the northward heat transport by the Atlantic Ocean.
776 *Boreas* **30**: 2-16.
- 777 Duplessy JC, Cortijo E, Ivanova E, Khusid T, Labeyrie L, Levitan M, Murdmaa I, Paterne M.
778 2005. Paleoceanography of the Barents Sea during the Holocene. *Paleoceanography* **20**:
779 A4004.
- 780 Ellingsen I, Slagstad D, Sundfjord A. 2009. Modification of water masses in the Barents Sea
781 and its coupling to ice dynamics: A model study. *Ocean Dynamics* **59**: 1095-1108.
- 782 Fahl K, Stein R. 2012. Modern seasonal variability and deglacial/Holocene change of central
783 Arctic Ocean sea ice cover: New insights from biomarker proxy records. *Earth Planetary*
784 *Science Letters* **351-352**: 123-133.
- 785 Fairbanks RG. 1989. A 17 000-year glacia-eustatic sea level record: Influence of glacial melting
786 rates on the Younger Dryas event and deep-ocean circulation. *Nature* **342**: 637-642.
- 787 Farmer EJ, Chapman MR, Andrews JE. 2008. Centennial-scale Holocene North Atlantic
788 surface temperatures from Mg/Ca ratios in *Globigerina bulloides*. *Geochemistry, Geophysics,*
789 *Geosystems* **9**: Q12029.
- 790 Forcino FL. 2012. Multivariate assessment of the required sample size for community
791 paleoecological research. *Palaeogeography, Palaeoclimatology, Palaeoecology* **315-316**: 134-
792 141.
- 793 Gammelsrød T, Leikvin Ø, Lien V, Budgell WP, Loeng H, Maslowski W. 2009. Mass and heat
794 transports in the NE Barents Sea: Observations and models. *Journal of Marine Systems* **75**: 56-
795 69.

- 796 Hald M, Andersson C, Ebbesen H, Jansen E, Klitegaard-Kristensen D, Risebrobakken B,
797 Salomonsen GR, Sejrup HP, Sarnthein M, Telford R. 2007. Variations in temperature and
798 extent of Atlantic water in the northern North Atlantic during the Holocene. *Quaternary Science*
799 *Reviews* **26**: 3423-3440.
- 800 Hebbeln D, Henrich R, Baumann KH. 1998. Paleoceanography of the last glacial/interglacial
801 cycle in the Polar North Atlantic. *Quaternary Science Reviews* **17**: 125-153.
- 802 Henrich R, Baumann KH, Huber R, Meggers H. 2002. Carbonate preservation records of the
803 past 3 Myr in the Norwegian-Greenland Sea and the northern North Atlantic: Implications for
804 the history of NADW production. *Marine Geology* **184**: 17-39.
- 805 Hopkins TS. 1991. The GIN Sea: A synthesis of its physical oceanography and literature
806 review, 1972–1985. *Earth-Science Reviews* **30**: 175-318.
- 807 Ivanov VV, Alexeev VA, Repina I, Koldunov NV, Smirnov A. 2012. Tracing Atlantic water
808 signature in the Arctic Sea ice cover East of Svalbard. *Advances in Meteorology* **2012**: 201818,
809 11.
- 810 Jakobsson M, Grantz A, Kristoffersen Y, Macnab R. 2004. Physiography and bathymetry of
811 the Arctic Ocean. In *The Organic Carbon Cycle in the Arctic Ocean*, Stein R, Macdonald RW
812 (eds). Springer: New York; 1-5.
- 813 Jernas P, Klitgaard Kristensen D, Husum K, Wilson L, Koç N. 2013. Palaeoenvironmental
814 changes of the last two millennia on the western and northern Svalbard shelf. *Boreas* **42**: 236-
815 255.
- 816 Johannessen T, Jansen E, Flatøy A, Ravelo AC. 1994. The relationship between surface water
817 masses, oceanographic fronts and plaeoclimatic proxies in surface sediments of the Greenland,
818 Iceland, Norwegian Seas. In *Carbon Cycling in the Glacial Ocean: Constraints of the Ocean's*
819 *Role in Global Change*, Zahn R, Pedersen TF, Kaminski MA, Labeyrie L (eds). Springer:
820 Berlin, 61-86.
- 821 Jonkers L, Brummer G-JA, Peeters FJC, van Aken HM, De Jong MF. 2010. Seasonal
822 stratification, shell flux, and oxygen isotope dynamics of left-coiling *N. pachyderma* and *T.*
823 *quinqueloba* in the western sub polar North Atlantic. *Paleoceanography* **25**: PA2204.
- 824 Katz ME, Cramer BS, Franzese A, Hönisch B, Miller KG, Rosenthal Y, Wright J. 2010.
825 Traditional and emerging geochemical proxies in foraminifera. *Journal of Foraminiferal*
826 *research* **40(2)**:165-192.
- 827 Kaufman D, Ager TA, Anderson NJ, Anderson PM, Andrews JT, Bartlein PJ, Brubakker LB,
828 Coats LL, Cwynar LC, Duvall ML, Dyke AS, Edwards ME, Eisner WR, Gajewski K,
829 Geirsdottir A, Hu FS, Jennings AE, Kaplan MR, Kerwin MW, Loshkin AV, MacDonald GM,
830 Miller GH, Mock CJ, Oswald WW, Otto-Bliesner BL, Porinchu DF, Rühland K, Smol JP, Steig
831 EJ, Wolfe BB. 2004. Holocene thermal maximum in the western Arctic (0 - 180 °N).
832 *Quaternary Science Reviews* **23**: 529-560.
- 833 Kaufman DS, Schneider DP, McKay NP, Ammann CM, Bradley RS, Briffa KR, Miller GH,
834 Otto-Bliesner BL, Overpeck JT, Vinther BM. 2009. Recent warming reverses long-term arctic
835 cooling. *Science* **325(5945)**: 1236-1239.
- 836 Keigwin LD, Boyle EA. 1989. Late Quaternary paleochemistry of high-latitude surface waters.
837 *Palaeogeography, Palaeoclimatology, Palaeoecology* **73**: 85-106.

- 838 Klitgaard Kristensen D, Rasmussen TL, Koç N. 2013. Paleoceanographic changes in the
839 northern Barents Sea during the last 16 000 years – new constraints on the last deglaciation of
840 the Svalbard-Barents Ice Sheet. *Boreas* **42**: 798-813.
- 841 Knies J, Cabedo-Sanz P, Bel, ST, Baranwal S, Fietz S, Rosell-Melé A. 2014. The emergence of
842 modern sea ice cover in the Arctic Ocean. *Nature Communications* **5**: 5608.
- 843 Knudsen KL. 1998. Foraminiferer i Kvartær stratigrafi: Laboratorie og fremstillingsteknik samt
844 udvalgte eksempler. *Geologisk Tidsskrift* **3**: 1-25.
- 845 Koç N, Jansen E, Haflidason H. 1993. Paleoceanographic reconstructions of surface ocean
846 conditions in the Greenland, Iceland and Norwegian seas through the last 14 ka based on
847 diatoms. *Quaternary Science Reviews* **12**: 115-140
- 848 Kohfeld KE, Fairbanks RG, Smith SL. 1996. *Neogloboquadrina pachyderma* (sinistral coiling)
849 as paleoceanographic tracers in polar oceans: Evidence from northeast water polynya plankton
850 tows, sediments traps, and surface sediments. *Paleoceanography* **11**: 679-699.
- 851 Kwok R. 2009. Outflow of Arctic Ocean sea ice into the Greenland and Barents Seas: 1979-
852 2007. *Journal of Climate* **22(9)**: 2438-2457.
- 853 Kwok R, Maslowski W, Laxon S. 2005. On large outflows of Arctic sea-ice into the Barents
854 Sea. *Geophysical Research Letters* **32**: L22503.
- 855 Laskar J, Robutel P, Joutel F, Gastineau M, Correia ACM, Levrard B. 2004. A long-term
856 numerical solution for the insolation quantities of the Earth. *Astronomy and Astrophysics* **428**:
857 261-285.
- 858 Loeng H. 1991. Features of the physical oceanographic conditions of the Barents Sea. *Polar
859 Research* **10**: 5-18.
- 860 Loeng H, Ozhigin V, Ådlandsvik B, Sagen H. 1993. *Current Measurements in the northeastern
861 Barents Sea*, International Council for the Exploration of the Sea, Council Meeting 1993/C:41,
862 Hydrographic Committee; 22.
- 863 Lubinski DJ, Polyak L, Forman SL. 2001. Freshwater and Atlantic water inflows to the deep
864 northern Barents and Kara seas since ca 13 ¹⁴Cka: foraminifera and stable isotopes. *Quaternary
865 Science Reviews* **20**: 1851-1879.
- 866 Mangerud J, Bondevik S, Gulliksen S, Hufthammer AK, Høisæter T. 2006. Marine ¹⁴C
867 reservoir ages for 19th century whales and molluscs from the North Atlantic. *Quaternary
868 Science Reviews* **25**: 3228-3245.
- 869 Manley TO. 1995. Branching of Atlantic Water within the Greenland-Spitsbergen Passage: An
870 estimate of recirculation. *Journal of Geophysical Research* **100**: 20627-20634.
- 871 Massé G, Rowland SJ, Sicre M-A, Jacob J, Jansen E, Belt ST. 2008. Abrupt climate changes
872 for Iceland during the last millennium: Evidence from high resolution sea ice reconstructions.
873 *Earth and Planetary Science Letters* **269**: 565-569.
- 874 Méheust M, Fahl K, Stein R. 2013. Variability in modern sea surface temperature, sea ice and
875 terrigenous input in the sub-polar North Pacific and Bering Sea: Reconstruction from biomarker
876 data. *Organic Geochemistry* **57**: 54-64.

- 877 Méheust M, Stein R, Fahl K, Max L, Riethdorf J-R. 2015. High-resolution IP₂₅-based
878 reconstruction of sea ice variability in the western North Pacific and Bering Sea during the past
879 18,000 years. *GeoMarine Letters* **36**: 101-111.
- 880 Midttun L. 1985. Formation of dense bottom water in the Barents Sea. *Deep-Sea Research* **32**:
881 1233-1241.
- 882 Müller J, Massé G, Stein R, Belt ST. 2009. Variability of sea ice conditions in the Fram Strait
883 over the past 30000 years. *Nature Geoscience* **2(11)**: 772-776.
- 884 Müller J, Wagner A, Fahl K, Stein R, Prange M, Lohman G. 2011. Towards quantitative sea
885 ice reconstructions in the northern North Atlantic: A combined biomarker and numerical
886 modelling approach. *Earth and Planetary Science Letters* **306**: 137-148.
- 887 Müller J, Werner K, Stein R, Fahl K, Moros M, Jansen E. 2012. Holocene cooling culminates
888 in sea ice oscillations in Fram Strait. *Quaternary Science Reviews* **47**: 1-14.
- 889 Müller J, Stein R. 2014. High-resolution record of late glacial sea ice changes in Fram Strait
890 corroborates ice-ocean interactions during abrupt climate shifts. *Earth and Planetary Science*
891 *Letters* **403**: 446-455.
- 892 National Snow and Ice Data Center (NSIDC), Boulder Colorado, www.nsidc.com
- 893 Navarro-Rodriguez A, Belt ST, Knies J, Brown TA. 2013. Mapping recent sea ice conditions
894 in the Barents Sea using the proxy biomarker IP₂₅: Implications for palaeo sea ice
895 reconstructions. *Quaternary Science Reviews* **79**: 26-39.
- 896 Novitskiy VP. 1961. Permanent currents of the northern Barents Sea. *Trudy Gosudarstvennogo*
897 *Okeanograficheskogo Instituta* **64**: 1-32. (English Translation).
- 898 Oppo DW, Fairbanks RG. 1989. Carbon isotope composition of tropical surface water during
899 the past 22,000 years. *Paleoceanography* **4**: 333-351.
- 900 Pados T, Spielhagen RF. 2014. Species distribution and depth habitat of recent planktic
901 foraminifera in Fram Strait, Arctic Ocean. *Polar Research* **33**: 22483.
- 902 Pfirman SL, Bauch D, Gammelsrød T. 1994. The Northern Barents Sea: water mass distribution
903 and modification. In *The Polar Oceans and Their Role in Shaping the Global Environment*,
904 Johannessen OM, Muench RD, Overland JE (eds). *AGU Geoph. Monog. Series.*, **85**: 77-94.
- 905 Pfuhl HA, Shackleton NJ. 2004. Two proximal, high-resolution records of foraminiferal
906 fragmentation and their implications for changes in dissolution. *Deep-Sea Research Pt. I* **51**:
907 809-832.
- 908 Polyak L, Belt ST, Cabedo-Sanz P, Yamamoto M, Park YH. 2016. Holocene sea-ice conditions
909 and circulation at the Chukchi-Alaskan margin, Arctic Ocean, inferred from biomarker proxies.
910 *The Holocene* **26**: 1810-1821.
- 911 Rasmussen TL, Thomsen E, Slubowska MA, Jessen S, Solheim A, Koç N. 2007.
912 Paleoceanographic evolution of the SW Svalbard margin (76 °N) since 20 000 ¹⁴C yr BP.
913 *Quaternary Research* **67**: 100-114.
- 914 Reimer PJ, Baillie MGL, Bard E, Bayliss A, Beck JW, Blackwell PG, Ramsey CB, Buck CE,
915 Burr GS, Edwards RL, Friedrich HM, Grootes PM, Guilderson TP, Hajdas I, Heaton TJ, Hogg

- 916 AG, Hughen KA, Kaiser KF, Kromer B, McCormac FG, Manning SW, Reimer RW, Richards
917 DA, Southon JR, Talamo S, Turney CSM, Van Der Plicht J, Weyhenmeyer CE. 2009. IntCal09
918 and Marine09 radiocarbon age calibration curves, 0-50 000 years cal BP. *Radiocarbon* **51**:
919 1111-1150.
- 920 Renssen H, Goosse H, Muscheler R. 2006. Coupled climate model simulation of Holocene
921 cooling events: oceanic feedback amplifies solar forcing. *Climate of the Past* **2**: 79-90.
- 922 Risebrobakken B, Morros M, Ivanova EV, Chistyakova N, Rosenberg R. 2010. Climate and
923 oceanographic variability in the SW Barents Sea during the Holocene. *The Holocene* **20**: 609-
924 621.
- 925 Risebrobakken B, Dokken T, Smedsrud LH, Andersson C, Jansen E, Moros M, Ivanova EV.
926 2011. Early Holocene temperature variability in the Nordic Seas: The role of oceanic heat
927 advection versus changes in orbital forcing. *Paleoceanography* **26**: PA4206.
- 928 Rudels B. 1987. On the mass balance of the Polar Ocean, with special emphasis on the Fram
929 Strait. *Norsk Polarinstitutt Skrifter* **188**: 53.
- 930 Rudels B, Korhonen M, Schauer U, Pisarev S, Rabe B, Wisotzki A. 2014. Circulation and
931 transformation of Atlantic water in the Eurasian Basin and the contribution of the Fram Strait
932 inflow branch to the Arctic Ocean heat budget. *Progress in Oceanography* **132**: 128-152.
- 933 Sakshaug E, Bjørge A, Gulliksen B, Loeng H, Mehlum F. 1992. *Økosystem Barentshavet*.
934 Norges Allmenvitenskapelige Forskningsråd, Norges Fiskeriforskningsråd,
935 Miljøverndepartementet, 304.
- 936 Sarnthein M, Van Kreveld S, Erlenkeuser H, Grootes PM, Kucera M, Pflaumann U, Schulz M.
937 2003. Centennial-to-millennial-scale periodicities of Holocene climate and sediment injections
938 off the western Barents shelf, 75 °N. *Boreas* **32**: 447-461.
- 939 Schauer U, Loeng H, Rudels B, Ozhigin VK, Dieck W. 2002. Atlantic Water flow through the
940 Barents and Kara Seas. *Deep-Sea Research Pt. I* **49**: 2281-2298.
- 941 Screen JA, Simmonds I. 2010. The central role of diminishing sea ice in recent Arctic
942 temperature amplification. *Nature* **464**: 1334-1337.
- 943 Serreze MC, Francis JA. 2006. The arctic amplification debate. *Climate Change* **76(3-4)**: 241-
944 264.
- 945 Serreze M, Barrett A, Slater A, Steele M, Zhang J, Tenberth K. 2007. The large-scale energy
946 budget of the Arctic. *Journal of Geophysical Research* **112**: D11122.
- 947 Shimada K, Kamoshida T, Itoh M, Nishino S, Carmack E, McLaughlin F, Zimmermann S,
948 Proshutinsky A. 2006. Pacific Ocean inflow: Influence on catastrophic reduction of sea ice
949 cover in the Arctic Ocean. *Geophysical Research Letters* **33**: L08605
- 950 Simstich J, Sarnthein M, Erlenkeuser H. 2003. Paired $\delta^{18}\text{O}$ signals of *N. pachyderma* (s) and *T.*
951 *quinqueloba* show thermal stratification structure in the Nordic Seas. *Marine*
952 *Micropaleontology* **48**: 107-125.
- 953 Skirbekk K, Klitgaard Kristensen D, Rasmussen TL, Koç N, Forwick M. 2010. Holocene
954 climate variations at the entrance to a warm Arctic fjord: evidence from Kongsfjorden trough,
955 Svalbard. *Geological society, London, Special Publications 2010* **344**: 289-304.

- 956 Slubowska MA, Koç N, Rasmussen TL, Klitgaard-Kristensen D. 2005. Changes in the flow of
957 Atlantic water into the Arctic Ocean since the last deglaciation: Evidence from the northern
958 Svalbard continental margin, 80N. *Paleoceanography* **20**: PA4014.
- 959 Smedsrud LH, Esau I, Ingvaldsen RB, Eldevik T, Haugan PM, Li C, Lien VS, Olsen A, Omar
960 AM, Otterå OH, Risebrobakken B, Sandø AB, Semenov VA, Sorokina SA. 2013. The role of
961 the Barents Sea in the Arctic climate system. *Reviews of Geophysics* **51(3)**: 415-449.
- 962 Smik L, Cabedo-Sanz P, Belt ST. 2016. Semi-quantitative estimates of paleo Arctic sea ice
963 concentration based on source-specific highly branched isoprenoid alkenes: A further
964 development of the PIP25 index. *Organic Geochemistry* **92**: 63-69.
- 965 Smith WO, Sakshaug E. 1990. Polar phytoplankton. In *Polar oceanography, Part B:
966 Chemistry, Biology and Geology*, Smith WO (ed). Academic Press: New York; 447-525.
- 967 Sorteberg A, Kvingsdal B. 2006. Atmospheric forcing on the Barents Sea winter ice extent.
968 *Journal of Climate* **19**: 4772-4784.
- 969 Spielhagen RF, Erlenkeuser H. 1994. Stable oxygen and carbon isotopes in planktic
970 foraminifera from the Arctic Ocean surface sediments: Reflection of the low salinity surface
971 water layer. *Marine Geology* **119**:227-250.
- 972 Spielhagen RF, Werner K, Aagaard-Sørensen S, Zamelczyk K, Kandiano E, Budeus G, Husum
973 K, Marchitto T, Hald M. 2011. Enhanced modern heat transfer to the Arctic by warm Atlantic
974 water. *Science* **331**: 450-453.
- 975 Stangeew E. 2001. *Distribution and isotopic composition of living planktonic foraminifera N.
976 pachyderma (sinistral) and T. quinqueloba in the high latitude North Atlantic*. Ph.D. thesis,
977 Math.-Naturwiss. Fak., Christian-Albrechts-Univ., Kiel, Germany. (Available at [http://e-
978 diss.uni-kiel.de/diss_464/pp](http://e-diss.uni-kiel.de/diss_464/pp)).
- 979 Stein R, Fahl K, Schade I, Manerung A, Wassmuth S, Niessen F, Nam S. 2016a. Holocene
980 variability in sea ice cover, primary production, and Pacific-Water inflow and climate change
981 in the Chukchi and East Siberian Seas (Arctic Ocean). *Journal of Quaternary Science* ISSN
982 0267-8179, DOI:10.1002/jqs.2929.
- 983 Stein R, Fahl K, Schreck M, Knorr G, Niessen F, Forwick M, Gebhardt C, Jensen L, Kaminski
984 M, Kopf A, Matthiessen J, Jokat W, Lohmann G. 2016b. Evidence for ice-free summers in the
985 late Miocene central Arctic Ocean. *Nature Communications* **7**: 11148.
- 986 Steinsund PI, Hald M. 1994. Recent carbonate dissolution in the Barents Sea:
987 Paleoceanographic applications. *Marine Geology* **117**: 303-316.
- 988 Stroeve J, Holland MM, Meier W, Scambos T, Serreze M. 2007. Arctic sea ice decline: Faster
989 than forecast. *Geophysical Research Letters* **34**:L09501.
- 990 Stroeve J, Serreze MC, Holland MM, Kay JE, Malanik J, Barrett AP. 2012. The Arctic's rapidly
991 shrinking sea ice cover: a research synthesis. *Climate Change* **110**:1005-1027.
- 992 Stuiver M, Reimer PJ. 1993. Extended ¹⁴C data base and revised CALIB 3.0 ¹⁴C age calibration
993 program. *Radiocarbon* **35**: 215-230.

- 994 Vare LL, Massé G, Gregory TR, Smart CW, Belt ST. 2009. Sea ice variations in the central
995 Canadian Arctic Archipelago during the Holocene. *Quaternary Science Reviews* **28**: 1354-
996 1366.
- 997 Vare LL, Massé G, Belt ST. 2010. A biomarker-based reconstruction of sea ice conditions for
998 the Barents Sea in recent centuries. *The Holocene* **20(4)**: 637-643.
- 999 Vinje TE. 1977. Sea ice conditions in the European sector of the marginal seas of the Arctic,
1000 1966-75. *Aarbok Norsk Polarinstitut* **1975**: 163-174.
- 1001 Vinje T. 2001. Anomalies and trends of sea ice extent and atmospheric circulation in the Nordic
1002 Seas during the period 1864-1998. *Journal of Climate* **14(3)**: 255-267.
- 1003 Volkmann R. 2000. Planktic foraminifers in the outer Laptev Sea and the Fram Strait: Modern
1004 distribution and ecology. *Journal Foraminiferal Research* **30**: 157-176.
- 1005 Wassmann P, Reigstad M, Haug T, Rudels B, Carroll ML, Hop H, Gabrielsen GW, Falk-
1006 Petersen S, Denisenko SG, Arashkevich E, Slagstad D, Pavlova O. 2006. Food webs and carbon
1007 flux in the Barents Sea. *Progress in Oceanography* **71**: 232-287.
- 1008 Wassmann P. 2011. Arctic marine ecosystems in an era of rapid climate change. *Progress in*
1009 *Oceanography* **90**: 1-17.
- 1010 Weckström K, Massé G, Collins LG, Hanhijärvi S, Bouloubassi I, Sicre M-A, Seidenkrantz M-
1011 S, Schmidt S, Andersen TJ, Andersen ML, Hill B, Kuijpers A. 2013. Evaluation of the sea ice
1012 proxy IP₂₅ against observational and diatom proxy data in the SW Labrador Sea. *Quaternary*
1013 *Science Reviews* **79**: 53-62.
- 1014 Werner K, Spielhagen RF, Bauch D, Hass HC, Kandiano E. 2013. Atlantic Water advection
1015 versus sea ice advances in the eastern Fram Strait during the last 9 ka: Multi proxy evidence for
1016 a two-phase Holocene. *Paleoceanography* **28**: 283-295.
- 1017 Werner K, Frank M, Teschner C, Müller J, Spielhagen RF. 2014. Neoglacial change in deep
1018 water exchange and increase of sea ice transport through eastern Fram Strait: evidence from
1019 radiogenic isotopes. *Quaternary Science Reviews* **92**: 190-207.
- 1020 Wilson LJ, Hald M, Godtlielsen F. 2011. Foraminiferal faunal evidence of twentieth-century
1021 Barents Sea warming. *The Holocene* **21(4)**: 527-537.
- 1022 Woodgate RA, Weingartner TJ, Lindsay R. 2010. The 2007 Bering Strait oceanic heat flux and
1023 anomalous Arctic sea-ice retreat. *Geophysical Research Letters* **37**: L01602.
- 1024 Xiao X, Fahl K, Stein R, 2013. Biomarker distributions in surface sediments from the Kara and
1025 Laptev seas (Arctic Ocean): indicators for organic-carbon sources and sea ice coverage.
1026 *Quaternary Science Reviews* **79**: 40-52.
- 1027 Xiao X, Fahl K, Müller J, Stein R. 2015a. Sea ice distribution in the modern Arctic Ocean:
1028 Biomarker records from trans-Arctic Ocean surface sediments. *Geochimica Cosmochimica*
1029 *Acta* **155**: 16-29.
- 1030 Xiao X, Stein R, Fahl K. 2015b. MIS 3 to MIS 1 temporal and LGM spatial variability in Arctic
1031 Ocean sea ice cover: Reconstruction from biomarkers. *Paleoceanography* **30**: 969-983.

- 1032 Yang S, Christensen JH. 2012. Arctic sea ice reduction and European cold winters in CMIP5
1033 climate change experiments. *Geophysical Research Letters* **39**: L20707.
- 1034 Zamelczyk K, Rasmussen TL, Husum K, Haflidason H, de Vernal A, Krogh Ravna E, Hald M,
1035 Hillaire-Marcel C. 2012. Paleooceanographic changes and calcium carbonate dissolution in the
1036 central Fram Strait during the last 20 ka yr. *Quaternary Research* **78**: 405-416
- 1037 Zamelczyk K, Rasmussen TL, Husum K, Hald M. 2013. Marine calcium carbonate preservation
1038 vs. climate change over the last two millennia in the Fram Strait: Implications for planktic
1039 foraminiferal paleostudies. *Marine Micropaleontology* **98**: 14-27.
- 1040 Årthun M, Eldevik T, Smedsrud LH, Skagseth Ø, Ingvaldsen R. 2012. Quantifying the
1041 influence of Atlantic heat on Barents Sea ice variability and retreat. *Journal of Climate* **25**:
1042 4736-4743.

1043 **Figure captions**

1044 Table 1. Depth-age model of NP05-11-70GC calibrated using Calib 6.1.1 (Stuiver and Reimer,
1045 1993), the Marine09 calibration curve (Reimer *et al.*, 2009) and a local reservoir age (ΔR) of
1046 105 ± 24 after Mangerud *et al.* (2006).

1047 Figure 1. The modern oceanography is presented on a bathymetric map of the Barents Sea area.
1048 The core location of NP05-11-70GC is indicated by a black star, whereas previously published
1049 records are indicated by number: (1) Risebrobakken *et al.* (2010), (2) Wilson *et al.* (2011), (3)
1050 Berben *et al.* (2014), (4) Rasmussen *et al.* (2007), (5) Müller *et al.* (2012); Werner *et al.* (2013),
1051 (6) Skirbekk *et al.* (2010); Jernas *et al.* (2013), (7) Müller *et al.* (2009), (8) Slubowska *et al.*
1052 (2005); Jernas *et al.* (2013), (9) Klitgaard Kristensen *et al.* (2013), (10) Lubinski *et al.* (2001),
1053 (11) Duplessy *et al.* (2001); (2005), (12) Risebrobakken *et al.* (2011), and (13) Duplessy *et al.*
1054 (2005). Northern Barents Sea Opening (NBSO), Barents Sea Opening (BSO), Barents Sea Exit
1055 (BSX). (a) The main surface currents (Hopkins, 1991). Atlantic Water (red): Norwegian
1056 Atlantic Current (NwAC), North Cape Current (NCaC), West Spitsbergen Current (WSC),
1057 Return Atlantic Current (RAC), Yermak Branch (YB) and Svalbard Branch (SB). Polar Water
1058 (blue): Bear Island Current (BIC) and East Spitsbergen Current (ESC). Coastal Water (black).
1059 (b) Seasonal sea ice margins (April (purple) and August (orange)) for the period 1981–2010
1060 (National Snow and Ice Data Centre (NSIDC) Boulder Colorado, www.nsidc.com). The
1061 observed sea ice margin for April (dotted) and August (dashed) from historical data for four
1062 sub-periods between 1870 and 2002: 1870–1920 (red), 1921–1961 (yellow), 1962–1988 (pink)
1063 and 1989–2002 (black) (Divine and Dick, 2006). (c) Temperature (black) and Salinity (grey)
1064 profile at the NP05-11-70GC core site (78.40° N, 32.42° E). Water masses are defined
1065 according Gammelsrød *et al.* (2009).

1066 Figure 2. Depth-age model of NP05-11-70GC. Calibrated radiocarbon ages versus depth with
1067 a linear interpolation between the dated levels. Error bars indicate the sampled depth intervals
1068 and a $2\text{-}\sigma$ error on the calibrated ages.

1069 Figure 3. Biomarker analysis versus cal a BP and core depth. The black diamonds on the Y-
1070 axis denote the AMS ^{14}C converted to calibrated radiocarbon ages. (a) Sea ice biomarker IP₂₅
1071 versus age. (b) Phytoplankton biomarker brassicasterol versus age. (c) Phytoplankton-derived
1072 HBI III biomarker versus age. Biomarker concentrations are normalized to total organic carbon
1073 (black) and to sediment mass (grey). (d) Total organic carbon versus age. (e) P_BIP₂₅ versus age.
1074 (f) P_{III}IP₂₅ versus age. $>5\%$ summer sea ice concentration (SuSIC) is also indicated when P_{III}IP₂₅
1075 exceeds a value of 0.8 (Smik *et al.*, 2016). (g) Estimated spring sea ice concentration (SpSIC)
1076 versus age.

1077 Figure 4. Planktic foraminiferal fauna and preservation indicator analysis versus cal a BP and
1078 core depth. The black diamonds on the Y-axis denote the AMS ^{14}C converted to calibrated
1079 radiocarbon ages. (a) Total planktic foraminiferal concentration versus age. (b) Planktic
1080 foraminiferal fragmentation versus age. (c) Mean shell weight of *N. pachyderma* versus age.
1081 (d-i) Species-specific relative abundance versus age.

1082 Figure 5. Stable isotopes analysis performed on *N. pachyderma* versus cal a BP and core depth.
1083 The black diamonds on the X-axis denote the AMS ^{14}C converted to calibrated radiocarbon
1084 ages. (a) $\delta^{18}\text{O}$ measurements corrected for ice volume effect after Fairbanks (1989) (black) and
1085 uncorrected $\delta^{18}\text{O}$ measurements (grey) versus age. (b) $\delta^{13}\text{C}$ measurements versus age.

1086 Figure 6. Multi-proxy analysis versus cal a BP and core depth. The black diamonds on the Y-
1087 axis denote the AMS ^{14}C converted to calibrated radiocarbon ages. (a) July insolation at 78° N

1088 (Laskar *et al.*, 2004) (note the reversed axis) versus age. (b) Sea ice biomarker IP₂₅ versus age.
1089 Concentrations are normalized to total organic carbon (black line) and to sediment mass (grey
1090 line). (c) P_{III}IP₂₅ versus age. >5% summer sea ice concentration (SuSIC) is also indicated when
1091 P_{III}IP₂₅ exceeds a value of 0.8 (Smik *et al.*, 2016). (d) Estimated spring sea ice concentration
1092 (SpSIC) versus age. (e) $\delta^{18}\text{O}$ measurements corrected for ice volume effect after Fairbanks
1093 (1989) versus age. (f) Relative abundance of *N. pachyderma* versus age. (g) Planktic
1094 foraminiferal concentration versus age. (b-d) The in dark grey highlighted period reflects
1095 decreased sea ice conditions, whereas the in light grey highlighted periods indicate increased
1096 sea ice conditions. (e-g) The in grey highlighted periods are characterized by an increased
1097 influence of Atlantic Water.

1098 Figure 7. Illustrations of the proposed seasonal sea ice scenarios at the NP05-11-70GC core
1099 location (black star). The shaded areas surrounding the dotted lines represent the proposed
1100 variability of the sea ice margin for March (black), April (purple) and August (orange), whereas
1101 the numbers indicate the core locations of previous studies: (1) Berben *et al.* (2014), (2) Müller
1102 *et al.* (2012), (3) Müller *et al.* (2009), (4) Klitgaard Kristensen *et al.* (2013), and (5) Duplessy
1103 *et al.* (2001). (a) Period I. (b) Period II. (c) Period III (dotted lines with shaded areas) and present
1104 day situation (full lines) based on mean sea ice margins (1981–2010) (National Snow and Ice
1105 Data Centre (NSIDC) Boulder Colorado, www.nsidc.com).

1106

1107 Table 1

1108

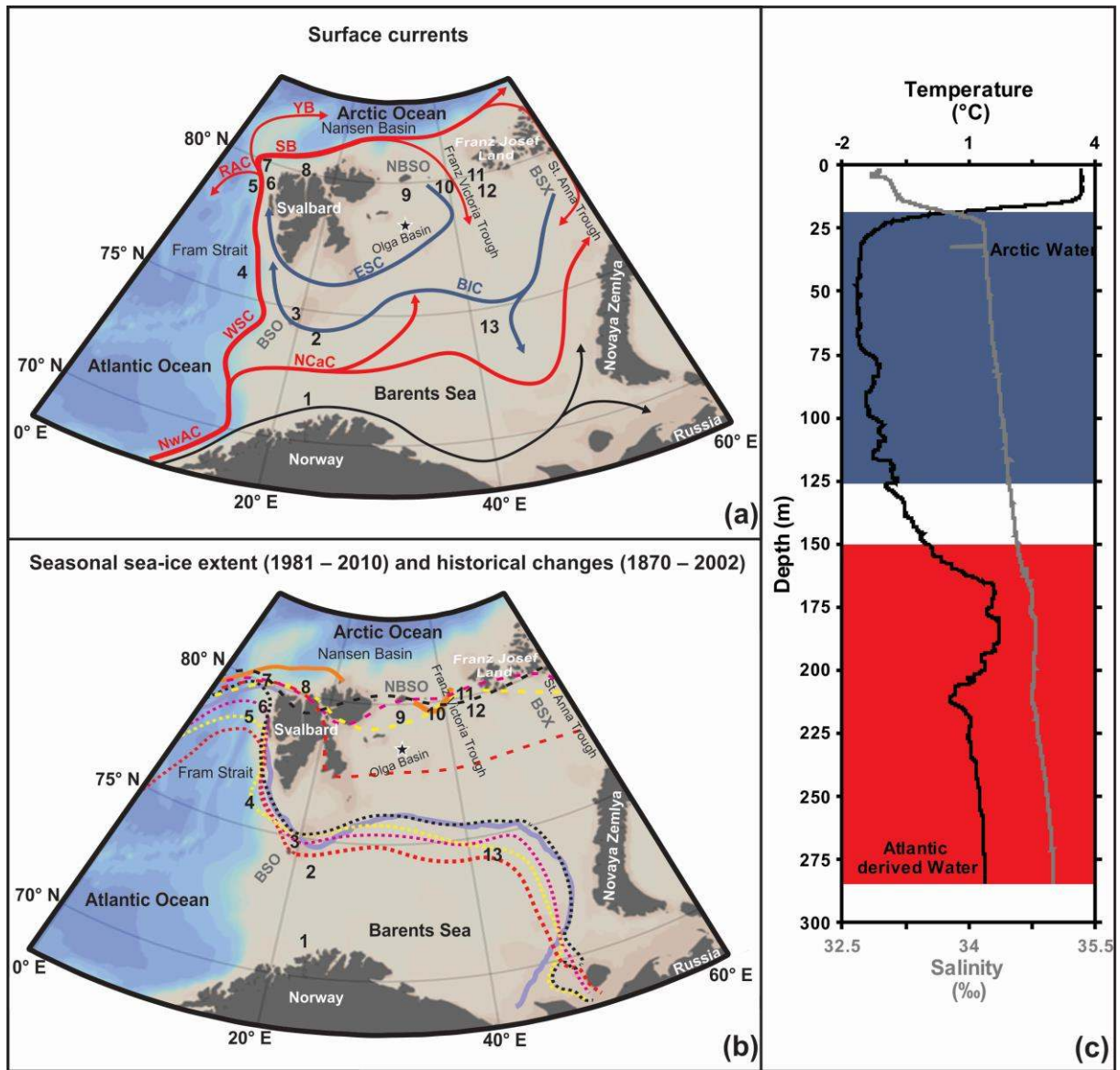
Lab ID	Core depth (cm)	Material	Uncorrected AMS ¹⁴C age	1σ	Calibrated age 2-σ range	Calibrated age used in depth-age model (cal a BP)
Beta-331327	37 - 43	Benthic foraminifera	2780	30	2281—2496	2389
Beta-346803	67 - 72	Benthic foraminifera	6110	40	6298—6536	6417
Beta-331328	122 - 127	Benthic foraminifera	8870	50	9307—9527	9417
Beta-331329	213 - 230	Benthic foraminifera	> 43500			

1109

1110

1111 Figure 1

1112

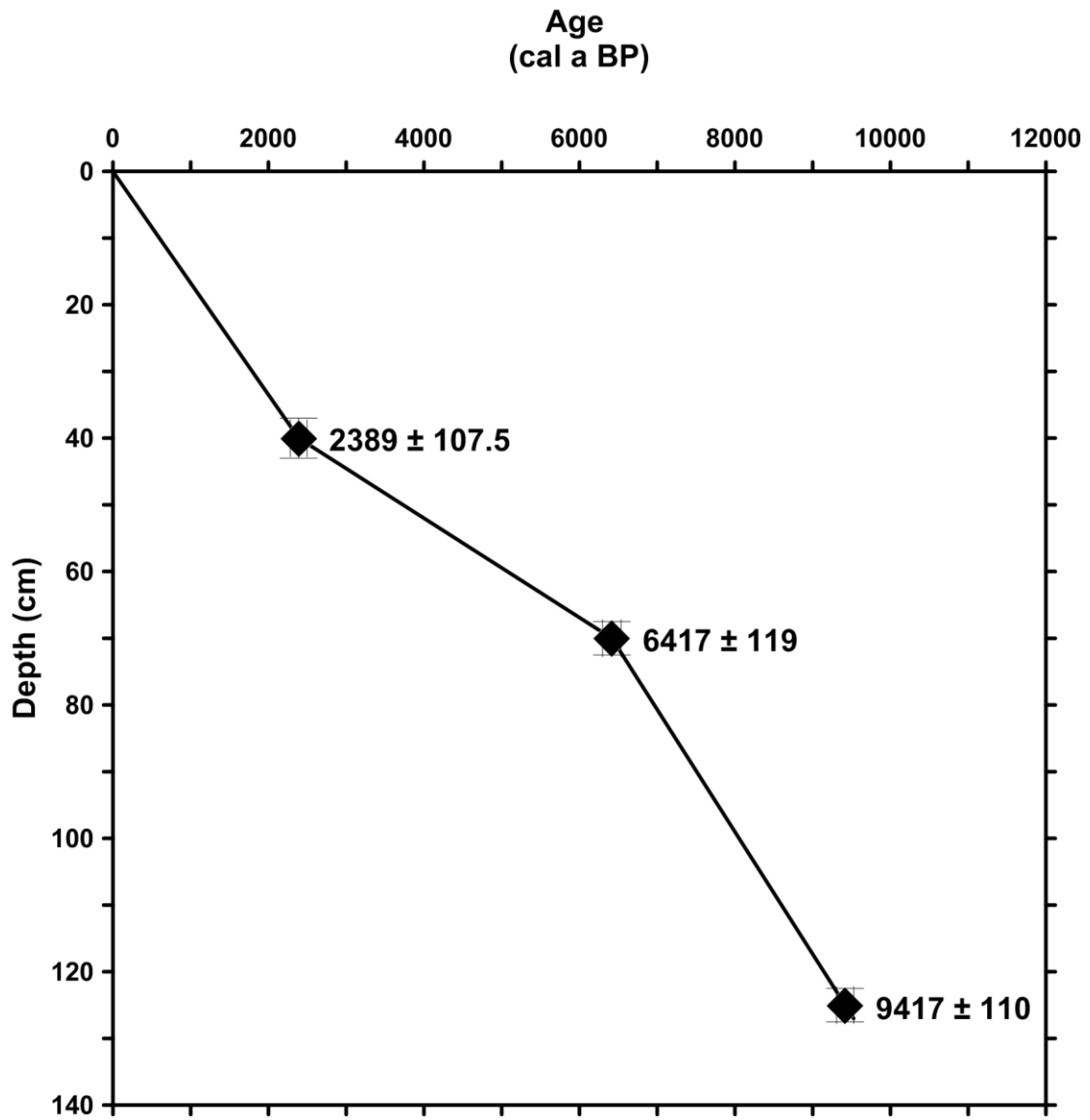


1113

1114

1115 Figure 2

1116

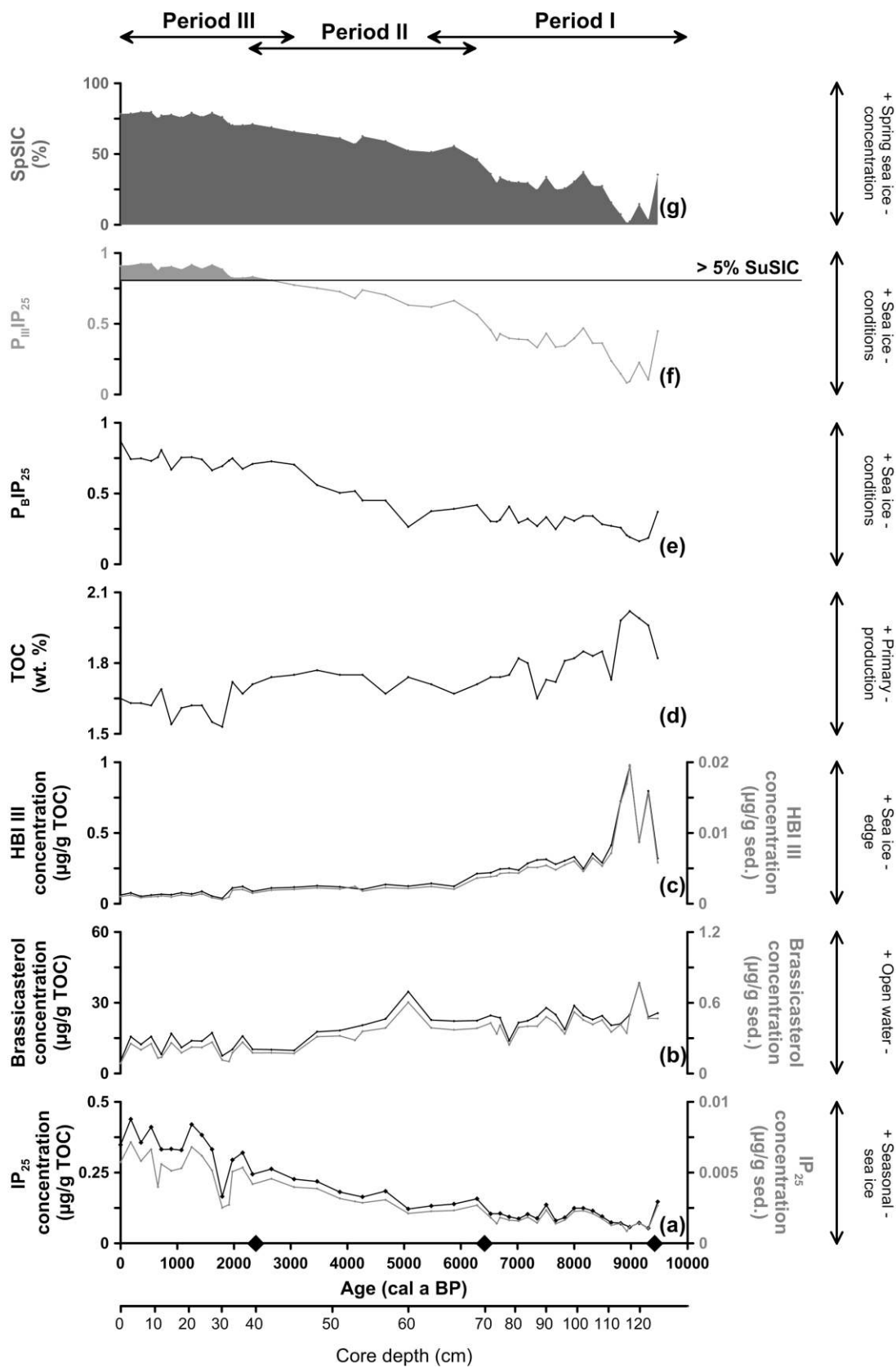


1117

1118

1119 Figure 3

1120

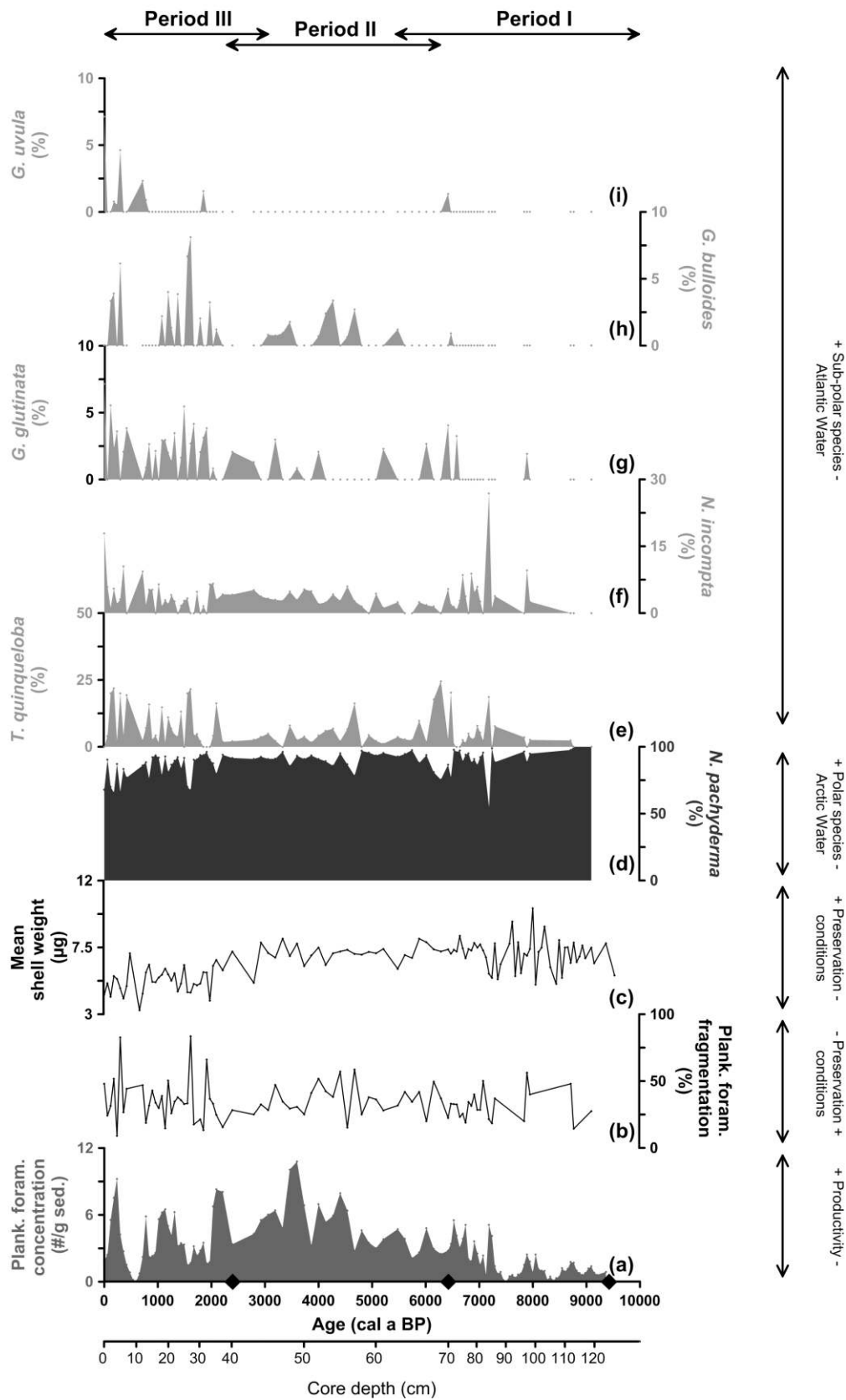


1121

1122

1123 Figure 4

1124

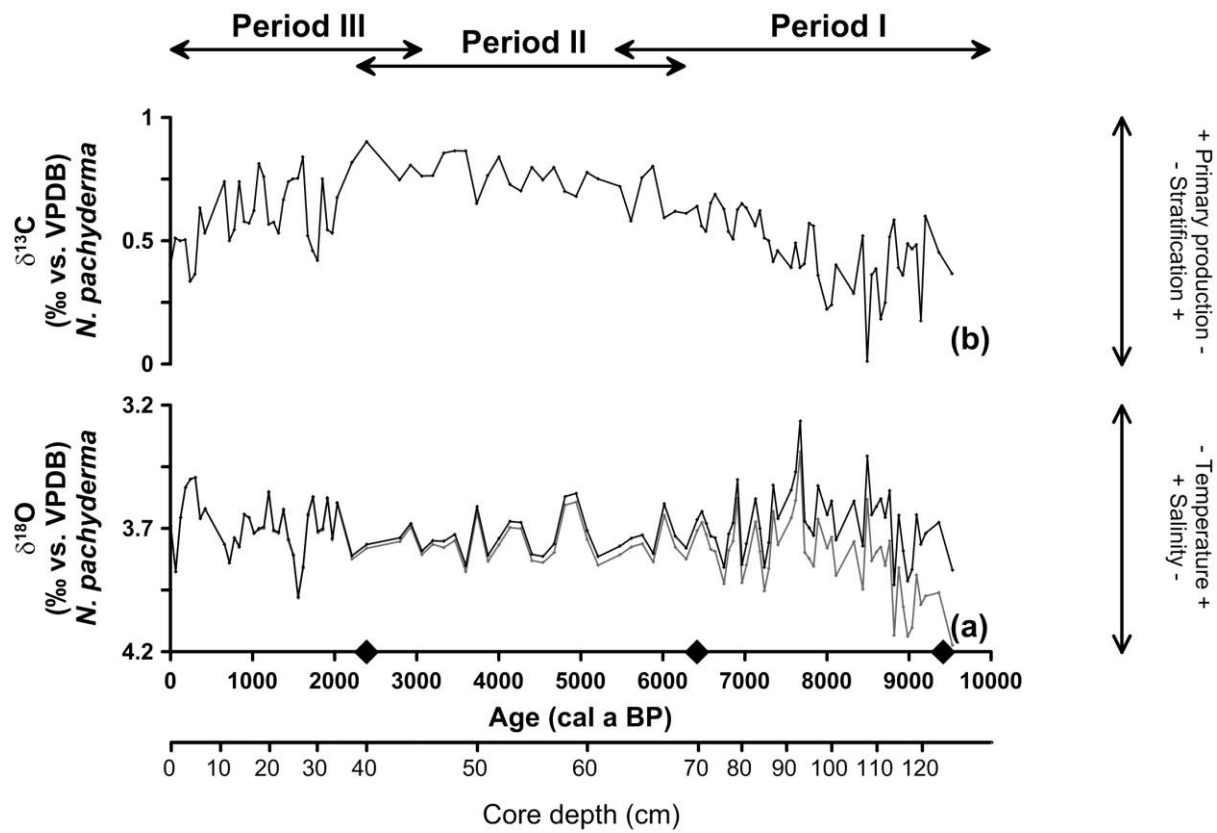


1125

1126

1127 Figure 5

1128

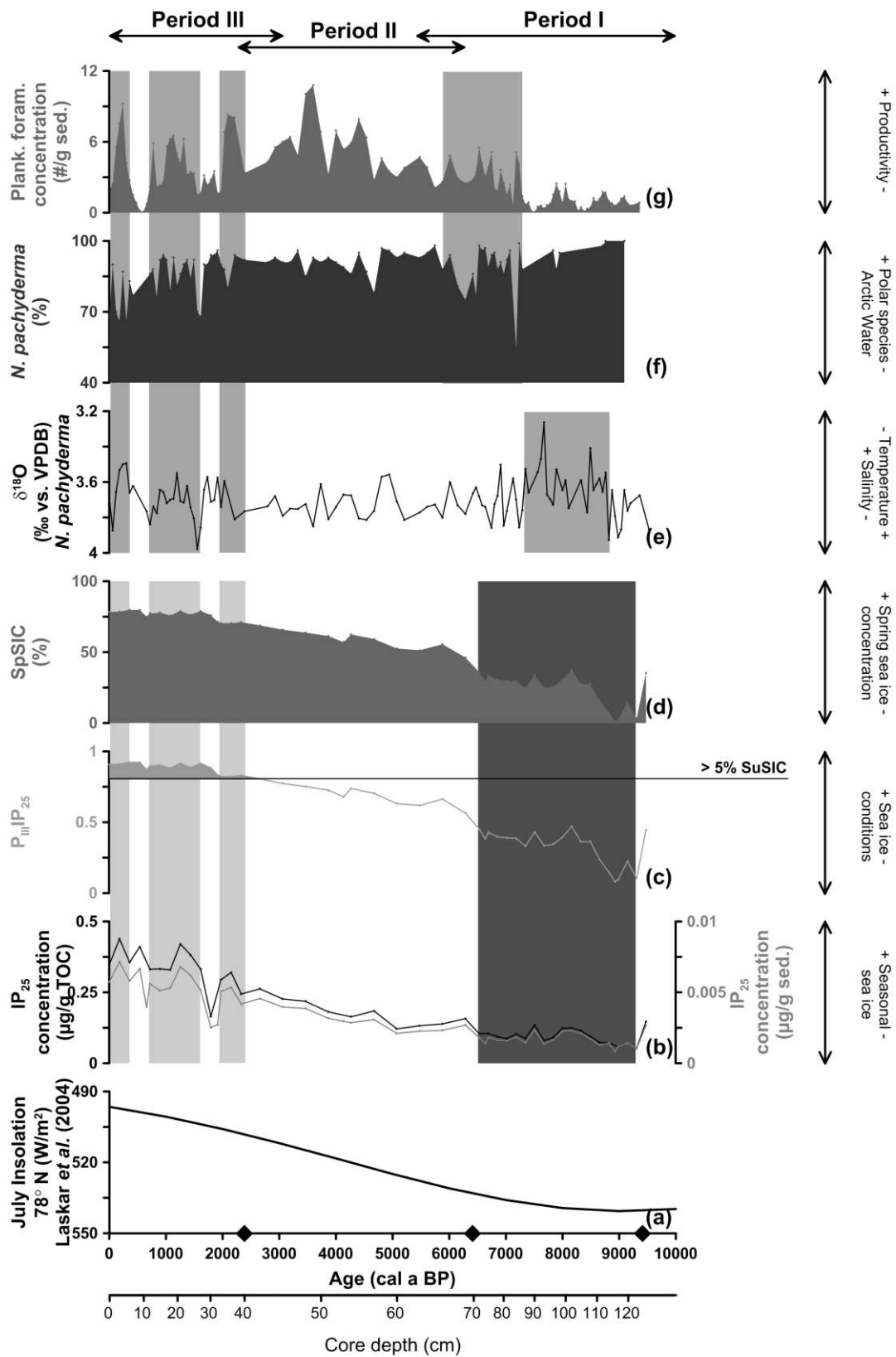


1129

1130

1131 Figure 6

1132

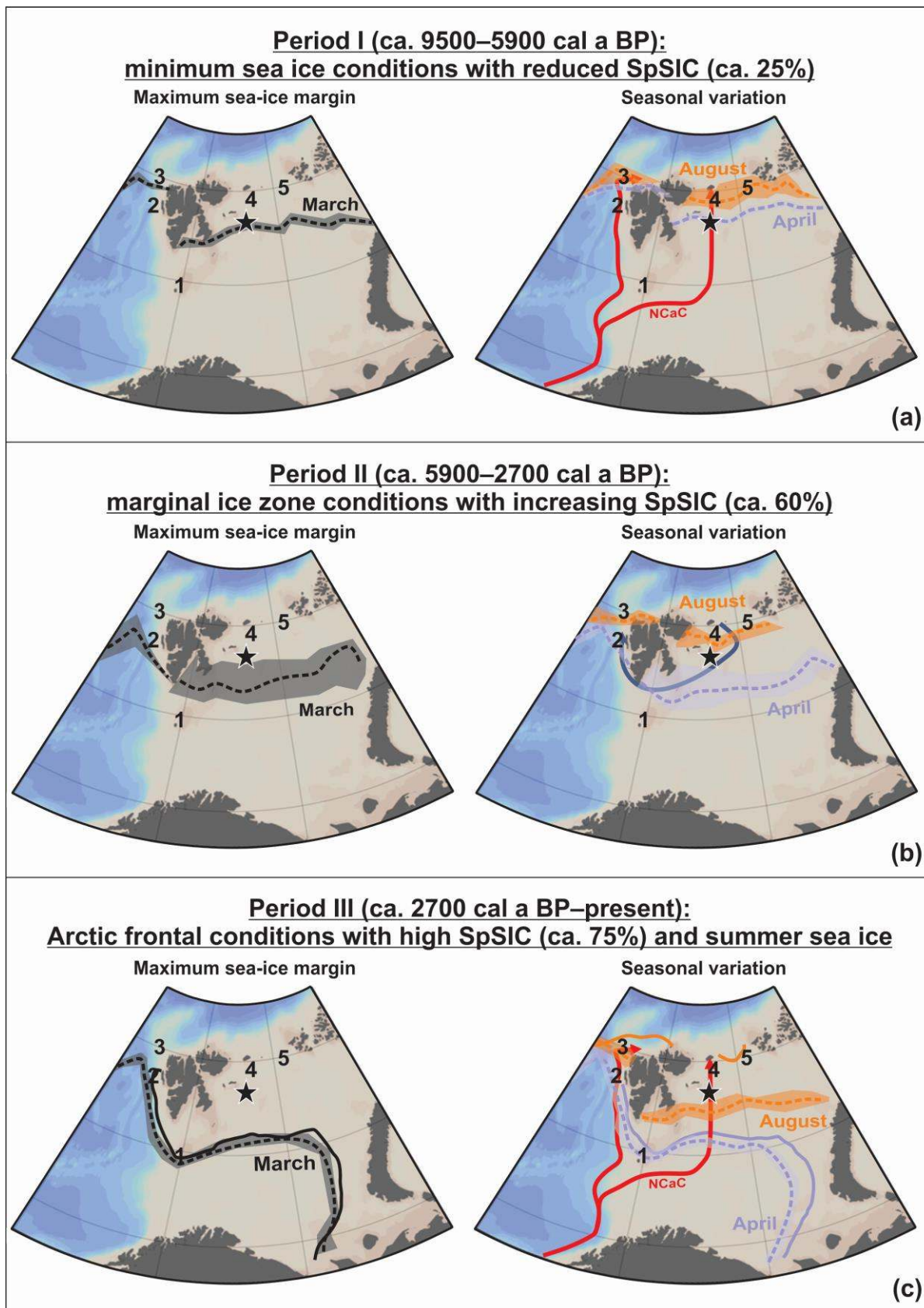


1133

1134

1135 Figure 7

1136



1137

1138